Critical dynamics at incommensurate phase transitions and NMR relaxation experiments

B. A. Kaufmann, F. Schwabl, and U. C. Täuber
Institut für Theoretische Physik, Physik-Department der Technischen Universität München, James-Franck-Straße, 85747 Garching, Germany
(October 30, 2013)

We study the critical dynamics of crystals which undergo a second-order phase transition from a high-temperature normal phase to a structurally incommensurate (IC) modulated phase. We give a comprehensive description of the critical dynamics of such systems, e.g. valid for crystals of the A_2BX_4 family. Using an extended renormalization scheme, we present a framework in which we analyze the phases above and below the critical temperature T_I. Above T_I, the crossover from the critical behavior to the mean-field regime is studied. Specifically, the resulting width of the critical region is investigated. In the IC modulated phase, we consider explicitly the coupling of the order parameter modes to one-loop order. Here the Goldstone anomalies and their effect on measurable quantities are investigated. We show their relation with the postulated phason gap. While the theory can be applied to a variety of experiments, we concentrate on quadrupole-perturbed nuclear magnetic resonance (NMR) experiments. We find excellent agreement with these dynamical measurements and provide answers for some questions that arose from recent results.

I. INTRODUCTION

This paper is concerned with the critical dynamics of crystals undergoing a second-order phase transition from a high-temperature normal (N) phase to a structurally incommensurate (IC) modulated phase. In the IC phase, the translational symmetry of the lattice is broken by a modulation in such a way that the characteristic wave vector $\mathbf{q}_I$ is a non-rational multiple of a basic lattice vector. The occurrence of incommensurate modulations is in general understood as a consequence of competing interactions.[1] The most important characteristic of these systems is that the ground state does not depend on the actual phase of the incommensurate modulation at a lattice site. This implies that the initial phase of the modulation wave is arbitrary and one must take into account a phase shift degeneration of the ground state energy. Consequently, not only the amplitude of the modulating vector is required to characterize each configuration, but in addition the phase at a arbitrary lattice site must be fixed. Therefore, a two-dimensional order parameter (OP) has to be employed in order to describe the phase transition from a N phase to an IC modulated phase.[2] Interesting static properties, e.g., the very rich phase diagrams of systems with competing interactions, emerge.[3]

However, in this work we concentrate on dynamical properties. Considering fluctuations of the OP, the normal modes can be expressed in terms of the transverse and longitudinal components $\psi^{\perp}$ and $\psi^{\parallel}$ in the two-dimensional OP space.[2] The fluctuations of $\psi^{\perp}$ and $\psi^{\parallel}$ can be identified with the fluctuations of the phase and the amplitude of the modulation in the crystal.[4] As a consequence of the OP being two-dimensional, the lattice dynamics of structurally incommensurate phases shows some peculiar effects which are different from ordinary crystalline phases. Namely, below the transition temperature T_I two non-degenerate branches of modes appear in the dynamical spectrum.[4] The "amplitudon" branch, connected with the fluctuations of the amplitude of the incommensurate modulation, exhibits common soft-mode behavior. In addition the "phason" branch represents the massless Goldstone modes of the system, here originating of the invariance of the crystal energy with respect to a phase shift. Because of the massless Goldstone modes[5,6] present in the entire IC phase, new types of anomalies may occur. Examples of such anomalies were discussed in the literature before.[7–10] Thus we expect some peculiar features of the dynamics in the IC modulated phase stemming from the Goldstone modes and their coupling to the other OP modes.

The purpose of this paper on the one hand is to provide a general framework for the analysis of the critical dynamics above and below the N/IC phase transition. The theoretical description of such systems is based on an $O(2)$ symmetric time-dependent Ginzburg-Landau model, with purely relaxational behavior of the non-conserved order parameter.[4] The more general $O(n)$-symmetric model has been widely studied above the critical temperature by means of the dynamical renormalization group.[11,12] Below the critical temperature, the $O(n)$ symmetry is spontaneously broken; as mentioned above parallel and perpendicular fluctuations have to be distinguished. We will start from the field-theoretical model of incommensurate phase transitions and derive the corresponding dynamical Janssen-De Dominicis functional,[13,14] which provides us with the framework to calculate interesting theoretical properties and correlations functions, which are required for the interpretation

of experimental data.

Furthermore, we intend to give a comprehensive theoretical description that goes beyond the mean-field or quasi-harmonic approach for the IC phase and which is missing to date. We present an explicit renormalization-group analysis to one-loop order above and below the critical temperature T_I. The renormalization group theory will lead us beyond the mean-field picture and provide some new insight on the effects of the Goldstone modes on the dynamical properties below T_I. Some specific features of the Goldstone modes were discussed for the statics by Lawrie[15] and for the dynamics in Refs. 16 and 10. In the present paper, we extend the analysis of the $O(n)$-symmetric model, specifically for the case $n = 2$. We also consider the crossover behavior from the classical critical exponents to the non-classical ones in detail, both above and below the critical temperature (see also Ref. 17).

Furthermore our model is employed to analyze specific experiments. Quadrupole-perturbed nuclear magnetic resonance (NMR) is an established method to investigate IC phases in a very accurate way.[18] In this probe, the interaction of the nuclear quadrupole moment (Q) of the nucleus under investigation with the electric field gradient (EFG) at its lattice site is measured. The fluctuations of the normal modes give rise to a fluctuating EFG, which is related to the transition probabilities between the nuclear spin levels. As a consequence, the relaxation rate $1/T_1$ of the spin-lattice relaxation is given by the spectral density of the EFG fluctuations at the Larmor frequency. We calculate the NMR relaxation rate with our theoretical model, and compare our findings with the experimental data. Our results may be used to interpret a variety of experimental findings; however, here we will restrict ourselves to the analysis of NMR experiments. The theory presented here is appropriate for the universality class containing, e.g., the crystals of the A_2BX_4 family. Some very precise NMR experiments on these crystals were performed over the past years.[18,19] Above T_I, these data can be used to analyze the critical dynamics in a temperature range of $T - T_I = 100K$ more closely. Below T_I, an identification of relaxation rates, caused by fluctuations of the amplitude and the phase, respectively, at special points of the NMR frequency distribution is possible. Therefore the relaxation rates $1/T_A$ and $1/T_\phi$, referring to the critical dynamics of the two distinct excitations ("amplitudons" and "phasons"), can be studied separately. These experiments led to some additional open questions. Above the critical temperature T_I, a large region was reported where non-classical critical exponents were found.[20] Below T_I, the presence of a phason gap is discussed in order to clarify some experiments as well as the theoretical understanding.[21,20] We will show how these questions can be resolved within the framework of our theory.

This paper is organized as follows: In the following section we introduce the model free energy for a system that reveals a N to IC phase transition. The dynamics of the amplitude and phase modes is described by Langevin-type stochastic equations of motion, and we give a brief outline of the general dynamical perturbation theory. In Sec. III, the connection between the NMR experiments and the susceptibility calculated within our theory is discussed. We shall see that the spectral density functions are closely related to the measured relaxation times. The high-temperature phase is analyzed in Sec. IV. Above T_I, scaling arguments are used to derive the critical exponents for the relaxation rate. The crossover from non-classical to classical critical behavior is discussed by means of a renormalization group analysis, and we comment on the width of the critical region. In Sec. V, we apply the renormalization group formalism to the low-temperature phase. The susceptibility, containing the critical dynamical behavior for the amplitudon and phason modes, is calculated to one-loop order. Specifically, the influence of the Goldstone mode is investigated. In the final section we shall discuss our results and give some conclusions.

II. MODEL AND DYNAMICAL PERTURBATION THEORY

A. Structurally incommensurate systems

We want to study second-order phase transitions from a high-temperature normal (N) phase to a structurally incommensurate (IC) modulated phase at the critical temperature T_I. The real-space displacement field corresponding to the one-dimensional incommensurate modulation can be represented by its normal mode coordinates $Q(\mathbf{q})$.[2] We will treat systems with a star of soft modes[22] consisting only of two wavevectors $\mathbf{q}_I$ and $-\mathbf{q}_I$ along one of the principal directions of the Brillouin zone, e.g. substances of the A_2BX_4 family.[2] Because the incommensurate modulation wave is in most cases, at least close to T_I, a single harmonic function of space, the primary Fourier components $\langle Q(\mathbf{q})\rangle \propto \delta(\mathbf{q} \pm \mathbf{q}_I)e^{i\phi_0}$ with the incommensurate wavevectors $\pm\mathbf{q}_I$ are dominating. Using $Q(\mathbf{q})$ as a primary order parameter of the normal-to-incommensurate phase transition in the Landau-Ginzburg-Wilson free energy functional, diagonalization leads to[2]

$$\begin{aligned} H[\{\psi_\circ^\alpha\}] =& \frac{1}{2}\sum_{\alpha=\phi,A}\int_{\mathbf{k}}(r_\circ + k^2)\psi_\circ^\alpha(\mathbf{k})\psi_\circ^\alpha(-\mathbf{k}) \\ &+ \frac{u_\circ}{4!}\sum_{\alpha,\beta=\phi,A}\int_{\mathbf{k}_1}\cdots\int_{\mathbf{k}_4} \\ &\times \psi_\circ^\alpha(\mathbf{k}_1)\psi_\circ^\alpha(\mathbf{k}_2)\psi_\circ^\beta(\mathbf{k}_3)\psi_\circ^\beta(\mathbf{k}_4)\,\delta(\sum_{l=1}^{4}\mathbf{k}_l)\ , \end{aligned} \tag{2.1}$$

with new Fourier coordinates $\psi_\circ^\phi(\mathbf{k})$ and $\psi_\circ^A(\mathbf{k})$ in the OP space. Here, we have introduced the abbreviations $\int_k ... = \frac{1}{(2\pi)^d}\int d^dk...$, and $\int_\omega ... = \frac{1}{2\pi}\int d\omega...$.

Below the phase transition, the fluctuations of $\psi_\circ^\phi$ and $\psi_\circ^A$ can be identified with the fluctuations of the phase and the amplitude of the displacement field, named *phason* and *amplitudon*.[4] The wavevector $\mathbf{k}$ indicates the derivation from the incommensurate wavevector $\mathbf{q_I}$,

$$\mathbf{k} = \mathbf{q} \mp \mathbf{q}_I \ . \tag{2.2}$$

The parameter $r_\circ$ is proportional to the distance from the mean-field critical temperature $T_{\circ I}$

$$r_\circ \propto T - T_{\circ I} \tag{2.3}$$

and the positive coupling $u_\circ$ gives the strength of the isotropic anharmonic term. Unrenormalized quantities are denoted by the suffix $\circ$.

The functional $H[\psi_\circ^\alpha]$ describes the statics of the normal-to-incommensurate phase transition. It represents the n-component isotropic Heisenberg model; in the case $n = 2$, it is also referred to as the XY model. For the sake of generality, the n-component order parameter case will be considered in the theoretical treatment.

B. Critical Dynamics

The critical dynamics of the system under consideration is characterized by a set of generalized Langevin equations for the "slow" variables, which in our case consist of the non-conserved order parameter fluctuations (because of the critical slowing-down in the vicinity of a phase transition).[23] The purely relaxational behavior[24] is described by the following Langevin-type equation of motion

$$\frac{\partial}{\partial t}\,\psi_\circ^\alpha(\mathbf{k},t) = -\lambda_\circ\,\frac{\delta H[\{\psi_\circ^\alpha\}]}{\delta\psi_\circ^\alpha(-\mathbf{k},t)} + \zeta^\alpha(\mathbf{k},t)\ . \tag{2.4}$$

The damping is caused by the fast degrees of freedom, which are subsumed in the fluctuating forces ζ^α. According to the classification by Halperin and Hohenberg, we are considering model A.[23]

The probability distribution for the stochastic forces ζ^α is assumed to be Gaussian. Therefore

$$\langle\zeta^\alpha(\mathbf{k},t)\rangle = 0, \tag{2.5}$$

$$\langle\zeta^\alpha(\mathbf{k},t)\,\zeta^\beta(\mathbf{k}',t')\rangle = 2\,\lambda_\circ\,\delta(\mathbf{k}-\mathbf{k}')\,\delta(t-t')\,\delta^{\alpha\beta}\ , \tag{2.6}$$

where the Einstein relation (2.6) guarantees that the equilibrium probability density is given by

$$P[\{\psi_\circ^\alpha\}] = \frac{e^{-H[\{\psi_\circ^\alpha\}]}}{\int\mathcal{D}[\{\psi_\circ^\alpha\}]e^{-H[\{\psi_\circ^\alpha\}]}}\quad . \tag{2.7}$$

Following the dynamical perturbation theory developed by Janssen[14] and De Dominicis,[13] we want to calculate the dynamical properties of our system, e.g. the dynamical correlation functions.

First, the stochastic forces are eliminated, using equation (2.4) and the Gaussian distribution for the stochastic forces ζ^α. After a Gaussian transformation and the introduction of auxiliary Martin-Siggia-Rose[25] fields $\tilde\psi_\circ^\alpha$, the non-linearities occuring in the initial functional are reduced. A perturbation theory analogous to the static theory can now be implemented on the basis of the path-integral formulation. We define the generating functional

$$Z[\{\tilde h^\alpha\},\{h^\alpha\}] \propto \int\mathcal{D}[\{i\tilde\psi_\circ^\alpha\}]\,\mathcal{D}[\{\psi_\circ^\alpha\}] \times e^{J[\{\tilde\psi_\circ^\alpha\},\{\psi_\circ^\alpha\}]+\int d^dx\int dt\,\sum_\alpha(\tilde h^\alpha\,\tilde\psi_\circ^\alpha+h^\alpha\,\psi_\circ^\alpha)}\ , \tag{2.8}$$

where the resulting Janssen-De Dominicis functional $J = J_0 + J_{int}$ is split into the harmonic part J_0 and the interaction part J_{int},

$$J_0[\{\tilde\psi_\circ^\alpha\},\{\psi_\circ^\alpha\}] = \int_k\int_\omega\sum_\alpha\Big[\lambda_\circ\,\tilde\psi_\circ^\alpha(\mathbf{k},\omega)\,\tilde\psi_\circ^\alpha(-\mathbf{k},-\omega) - \tilde\psi_\circ^\alpha(\mathbf{k},\omega)\left[i\omega+\lambda_\circ\,(r_\circ+k^2)\right]\psi_\circ^\alpha(-\mathbf{k},-\omega)\Big]\ , \tag{2.9}$$

$$J_{int}[\{\tilde\psi_\circ^\alpha\},\{\psi_\circ^\alpha\}] = \frac{-\lambda_\circ\,u_\circ}{6}\int_{q_i}\int_{\omega_i}\delta(\sum_i\mathbf{k}_i)\,\delta(\sum_i\omega_i) \times\sum_{\alpha\beta}\tilde\psi_\circ^\alpha(\mathbf{k}_1,\omega_1)\,\psi_\circ^\alpha(\mathbf{k}_2,\omega_2)\,\psi_\circ^\beta(\mathbf{k}_3,\omega_3)\,\psi_\circ^\beta(\mathbf{k}_4,\omega_4)\ . \tag{2.10}$$

The N-point Green functions $G_{\circ\,\tilde\psi_i^\alpha\psi_j^\alpha}(\mathbf{k},\omega)$ and cumulants G^c can be derived by appropriate derivatives of Z and $\ln Z$ with respect to the sources $\tilde h^\alpha$ and h^α . Thus the standard scheme of perturbation theory can be applied. Further details can be found in textbooks (Refs. 26,27) and in Refs. 14,16.

In addition we want to list some important relations that will be useful for the discussion. The dynamical susceptibility gives meaning to the auxiliary fields by noting that it can be represented as a correlation function between an auxiliary field and the order parameter field[14]

$$\chi_\circ^{\alpha\beta}(\mathbf{x},t;\mathbf{x}',t') = \left.\frac{\delta\langle\psi_\circ^\alpha(\mathbf{x},t)\rangle}{\delta\tilde h^\beta(\mathbf{x}',t')}\right|_{\tilde h^\beta=0} = \langle\psi_\circ^\alpha(\mathbf{x},t)\,\lambda_\circ\,\tilde\psi_\circ^\beta(\mathbf{x}',t')\rangle\ . \tag{2.11}$$

Its Fourier transform

$$\chi_\circ^{\alpha\beta}(\mathbf{k},\omega) = \lambda_\circ\,G_{\circ\,\tilde\psi^\alpha\psi^\beta}(\mathbf{k},\omega)\ . \tag{2.12}$$

is associated with the Green functions $G_{\circ\,\tilde\psi^\alpha\psi^\beta}$. The fluctuation-dissipation theorem relates the correlation function of the order parameter fields and the imaginary part of the response function[14]

$$G_{\circ\,\psi^\alpha\psi^\beta}(\mathbf{k},\omega) = 2\frac{\Im\chi_\circ^{\alpha\beta}(\mathbf{k},\omega)}{\omega}\ , \tag{2.13}$$

which will enter the calculation of the NMR relaxation rate. E.g., considering only the harmonic part J_0 of the

dynamical functional and carrying out the functional integration gives

$$G_{\circ\,\psi^\alpha\psi^\beta}(\mathbf{k},\omega) = \delta^{\alpha\beta}\frac{2\lambda_\circ}{[\lambda_\circ(r_\circ+k^2)]^2+\omega^2}\ . \qquad (2.14)$$

Finally we want to introduce the vertex functions $\Gamma_{\circ\,\tilde\psi^\alpha\psi^\beta}$, which are related to the cumulants through a Legendre transformation. For example[14,16]

$$G^c_{\circ\,\tilde\psi^\alpha\psi^\alpha}(\mathbf{k},\omega) = \frac{1}{\Gamma_{\circ\,\tilde\psi^\alpha\psi^\alpha}(-\mathbf{k},-\omega)}\ . \qquad (2.15)$$

The vertex functions are entering the explicit calculation of Z factors and the susceptibility in the renormalization group theory. The advantage of working with vertex functions is that they are represented by one-particle irreducible Feynman diagrams only.

III. NMR-EXPERIMENTS AND SPIN-LATTICE RELAXATION

Quadrupolar perturbed nuclear magnetic resonance (NMR) can be used to study the dynamics of phase transitions from a N to a IC modulated phase.[18] In this method the interaction between the nuclear quadrupole moment Q and the electric-field gradient (EFG) V is the dominant perturbation $\mathcal{H}_Q$ of the Zeeman Hamiltonian. Thus in the corresponding Hamiltonian

$$\mathcal{H} = \mathcal{H}_Z + \mathcal{H}_Q \qquad (3.1)$$

next to the dominating Zeeman term $\mathcal{H}_Z$ one has to consider the quadrupole interaction $\mathcal{H}_Q = \frac{1}{6}\sum_{j,k} Q_{jk}V_{jk}$ as a perturbation. The quadrupole moment operator Q_{jk} is coupled linearly to the EFG tensor V_{jk} at the lattice site.[28,29]
The fluctuations of V_{jk} can be expressed via order parameter fluctuations, because of the dominant linear coupling of the EFG to the order parameter[30,31]

$$\delta V_{ij}(\mathbf{x},t) = A_{1ij}[\delta\psi^A(t) + i\delta\psi^\phi(t)]e^{i\mathbf{kx}+\Phi_0} + c.c.\ . \qquad (3.2)$$

We now briefly sketch how the OP fluctuations determine the relaxation rate. The spin-lattice relaxation describes the return of the nuclear spin magnetization M in the direction of the external field back to its thermal equilibrium value following a radio frequency pulse.[32] During that time the energy of the spin system is transferred to single modes of the lattice fluctuations.[19] Because the EFG fluctuations can be written as OP fluctuations, the spin-lattice relaxation is determined by the spectral density functions of the local OP fluctuations at the Larmor frequency $\omega = \omega_L$. The transition probabilities for nuclei with spin $I = \frac{3}{2}$ in three dimensions are given by[32,33]

$$\frac{1}{T_1} = W\left(\pm\frac{3}{2}\leftrightarrow\pm\frac{1}{2}\right) = \frac{\pi^2}{3}\left[J(V_{xy},\omega_L)+J(V_{yz},\omega_L)\right]$$
$$\propto \int_{BZ}\frac{\Im\chi^{\alpha\beta}_\circ(\mathbf{k},\omega_L)}{\omega_L} = \int_0^\Lambda \frac{1}{2}\ k^2\ G_{\circ\,\psi^\alpha\psi^\beta}(\mathbf{k},\omega_L)dk\ , \qquad (3.3)$$

with the spectral density of the EFG fluctuations

$$J(V_{ij},\omega) = \int_{-\infty}^{\infty}\overline{V_{ij}(t){V_{ij}}^*(t+\tau)}e^{-i\omega\tau}d\tau\ . \qquad (3.4)$$

Measuring the spin-lattice relaxation thus yields information on the susceptibility of the local fluctuations of the order parameter.

The spin-lattice relaxation was studied in great detail by means of echo pulse methods both below and above T_I.[18,19] Below the critical temperature T_I, it is possible for the prototypic system Rb_2ZnCl_4 to identify the relaxation rates $1/T_1^A$ and $1/T_1^\phi$, dominated in the plane-wave limit by the amplitudon and phason fluctuations, respectively.[19] Therefore, the dynamical properties of the order parameter fluctuations can be studied below the phase transition as well, and separately for the two distinct excitations.

IV. HIGH-TEMPERATURE PHASE

In this section, the critical behavior of the incommensurate phase transition above T_I will be investigated. On the basis of scaling arguments and the use of critical exponents, calculated within the renormalization-group theory for the XY model in three dimensions and model A, the temperature dependence of the NMR relaxation rate is analyzed in the first subsection. Next we study the crossover scenario of the temperature dependence of the relaxation rate in the second subsection by means of the renormalization group theory. Comparison with experimental data is made, and we comment on the width of the critical region.

A. Scaling laws for the relaxation time

Above the phase transition, the thermodynamical average of the order parameter components is zero. Because the structure of the correlation function of the order parameter does not change dramatically above T_I (see section IV B) and the calculation of the relaxation rate $1/T_1$ involves the integration of the correlation function over all wavevectors, we will derive a form of the correlation function using scaling arguments. Thus we are able to discuss the universal features of the relaxation rate behavior when approaching T_I from above. In the harmonic approximation we immediately get the correlation

function, which turns out to be the propagator of our functional J_0, [see Eq. (2.14)]

$$\langle \psi_\circ^\alpha(\mathbf{k},t)\,\psi_\circ^\beta(\mathbf{k}',t')\rangle = \delta(\mathbf{k}+\mathbf{k}')\delta(\omega+\omega')\delta^{\alpha\beta}G_\circ(k,\omega)\ , \tag{4.1}$$

$$G_\circ(k,\omega) = \frac{2\lambda_\circ}{[\lambda_\circ(r_\circ+k^2)]^2+\omega^2}\ . \tag{4.2}$$

The suffix $\circ$ will be omitted in the following discussion of this subsection, because no renormalization will be considered here.

We want to exploit our knowledge about the critical region. The static scaling hypothesis for the static response function states

$$\chi(k) = A_\chi \cdot \hat{\chi}(x)\cdot k^{-2+\eta} \tag{4.3}$$

with the scaling function $\hat{\chi}$, a constant prefactor A_χ, the scaling variable $x=(k\xi)^{-1}$ (ξ denoting the correlation length), and the critical exponent η. Neglecting a frequency dependence for the kinetic coefficient (Lorentzian approximation), the dynamic scaling hypothesis for the characteristic frequency of the OP dynamics states

$$\omega_\varphi(k) \equiv \lambda(k)/\chi(k) \sim k^z\ , \tag{4.4}$$

and we can deduce

$$\lambda(k) = A_\lambda\cdot\hat{\lambda}(x)\cdot k^{z-2+\eta}\ , \tag{4.5}$$

with $\hat{\lambda}(x)$ being the scaling function for the kinetic coefficient and A_λ a constant prefactor. Notice that for fixed wavevector k Eq. 4.4 leads to[23]

$$\omega_\varphi(k) \sim \xi^{-z}\ . \tag{4.6}$$

The correlation function $G(k,\omega)$ can now be rewritten in scaling form

$$G(k,\omega) = \Lambda\cdot\frac{1}{k^{z+2-\eta}}\cdot\hat{f}(\hat{\omega},x)\ , \tag{4.7}$$

with

$$\Lambda = \frac{2\ A_\chi^2}{A_\lambda},\quad \hat{\omega} = \frac{A_\chi}{A_\lambda}\frac{\omega}{k^z},\quad x=\frac{1}{k\xi},$$
$$\hat{f}(\hat{\omega},x) = \hat{\chi}(x)\cdot\frac{\hat{\lambda}(x)/\hat{\chi}(x)}{[\hat{\lambda}(x)/\hat{\chi}(x)]^2+\hat{\omega}^2}\ , \tag{4.8}$$

where the Lorentzian line shape is retained. Above T_I, this not a very crucial approximation, because the shape of the correlation function does not change in a first-order renormalization group analysis, as we will see in the next section. To calculate the relaxation rate $1/T_1$, one has to evaluate the integral [see Eq. (3.3)]

$$\frac{1}{T_1} \propto \int_0^\Lambda \frac{1}{2}\ k^2\ G(k,\omega_L)dk \tag{4.9}$$
$$\propto \Lambda\cdot\int_{BZ} k^2dk\ k^{-z-2+\eta}\hat{f}(k\omega_L^{-1/z},k\xi)\ .$$

With $u=k\omega_L^{-1/z}$ and $v=k\xi$ we introduce new variables

$$\varrho = \sqrt{u^2+v^2} = k\sqrt{\omega_L^{-2/z}+\xi^2} \tag{4.10}$$

and

$$\tan\varphi = \frac{v}{u} = \frac{\xi}{\omega_L^{-1/z}}\ . \tag{4.11}$$

This leads to the relation

$$\frac{1}{T_1} = \Lambda\cdot\left(\sqrt{\omega_L^{-2/z}+\xi^2}\right)^{z-1-\eta}\ I_\varrho\left(\hat{f}(\varrho,\varphi)\right)\ , \tag{4.12}$$

where the integral I_ϱ does not contribute to the leading temperature dependence.

The temperature dependence of the relaxation rate can now easily be found in the limits where the Larmor frequency or the frequency, of the critical fluctuations, respectively, dominate the integral and its prefactor.

1. Fast-motion limit ($\omega_L/\omega_\varphi \ll 1$)

For temperatures very far above the critical temperature T_I, the characteristic frequency is larger than the Larmor frequency. Thus the temperature dependence of the OP fluctuations determines the temperature dependence of the relaxation rate; the value of the Larmor frequency should not play any role.[34] For the integral

$$\frac{1}{T_1} = \Lambda\cdot\left(\omega_L^{-2/z}\left[1+\left(\omega_L/\xi^{-z}\right)^{2/z}\right]\right)^{(z-1-\eta)/2}\cdot I_\varrho \tag{4.13}$$

we obtain with $\tan\varphi = \text{const.}$ [see Eq. 4.11]

$$\frac{1}{T_1} \propto \xi^{z-1-\eta} = \left(\frac{T-T_I}{T}\right)^{-\nu\cdot(z-1-\eta)}\ . \tag{4.14}$$

Taking the values for the critical exponents from Table I, we find

$$\frac{1}{T_1} \propto \left(\frac{T-T_I}{T}\right)^{-0.663}\ . \tag{4.15}$$

This can be compared with the experimental results for Rb_2ZnCl_4 by Holzer et al.[20], who found for the leading scaling behavior of the relaxation rate, following the temperature-independent region, the exponent -0.625.

2. Slow-motion limit ($\omega_L/\omega_\varphi \gg 1$)

In the vicinity of the critical temperature T_I critical slowing down will occur. This means that the characteristic frequency ω_φ is approaching zero and will fall below the value of the Larmor frequency.[34] Thus, the characteristic time scale of the OP fluctuations is slower than the experimental time scale. For the temperature dependence of the relaxation rate

$$\frac{1}{T_1} \propto \Lambda \cdot \left(\xi^2 \left[\left(\xi^{-z}/\omega_L\right)^{2/z} + 1\right]\right)^{(z-1-\eta)/2} \cdot I_\varrho \ ,$$

we now obtain

$$\frac{1}{T_1} \propto \omega_L^{-(z-1-\eta)/z} \cdot \text{const} \ . \tag{4.16}$$

Taking the values for the critical exponents from Table I again

$$\frac{1}{T_1} \propto \ \omega_L^{-0.49} \ . \tag{4.17}$$

This is in good agreement with the experimental result[20] for Rb_2ZnCl_4 that the value of the relaxation rate near T_I scales as $\omega_L^{-0.5}$ for different Larmor frequencies.

We want to stress that the transition from the fast- to the slow-motion limit is a property of the integral entering the calculation of the relaxation rate. Because the susceptibility is evaluated at fixed ω_L, there exists for a lower boundary for the integral $T \approx T_I$. This means that the transition from the temperature-dependent to the temperature independent behavior near T_I is fixed by the scale ω_L. It should also be mentioned that our results reproduce those obtained earlier by Holzer et al. (see Ref. 20), when the van Hove approximation for z is used ($z \approx 2$).

B. Renormalization-group analysis above T_I

Our investigations concerning the critical behavior above T_I in the last section led to fair agreement with experimental data. It was possible to gain the critical exponents for the frequency and temperature dependence of the relaxation rate in a quantitatively accurate way. Furthermore, we obtained a qualitative understanding of the transition of the relaxation rate $1/T_1$ from the slow- to the fast-motion limit. This transition is caused by the characteristic frequency of the order-parameter dynamics ω_φ approaching zero, i.e., the critical slowing down near T_I. This renders the Larmor frequency ω_L the dominating time scale, $1/T_1$ becomes temperature-independent near T_I.

At this point we want to consider what happens upon leaving the region near the transition temperature and going to higher temperatures. Our results (4.13) for the fast-motion limit are based on the assumption that fluctuations are very important. We used non-classical exponents and scaling arguments valid in the critical region. The question arises how large this region of temperature, where the system displays the non-classical behavior calculated in the last section, will be. Increasing temperature diminishes the effect of fluctuations. One would expect that at some temperature Gaussian behavior should emerge. We shall apply the renormalization group theory to one-loop approximation in order to describe the transition from the fluctuation-dominated behavior near T_I to a temperature region where the mean-field description should be valid. It is obvious that the properties of the integral, responsible for the transition between the slow and the fast motion limit, will account for the crossover of the leading scaling behavior when the temperature is increased. In order to discuss the crossover within this analysis a modified minimal-subtraction prescription is employed. This scheme was first introduced by Amit and Goldschmidt[35] and subsequently explored by Lawrie for the study of Goldstone singularities.[15] It can comprise exact statements in a certain limit. Below T_I, this is the regime dominated by the Goldstone modes alone; in the region above T_I, which we will consider in this section, the mean-field result is used. In this scheme, in addition the standard field-theoretical formulation of the renormalization group is neatly reproduced. Following the arguments of Schloms and Dohm[36] and Ref. 16 we can refrain from the ε expansion, with

$$\varepsilon = 4 - d \tag{4.18}$$

defining the difference from the upper critical dimension of the ϕ^4 model. This is motivated by the following. Above T_I the Gaussian or zero-loop theory becomes exact in the high-temperature limit. The critical fixed point, i.e., the Heisenberg fixed point, dominating the behavior of the system near the critical temperature is calculated to one-loop order. The main interest here lies in the crossover behavior between these two fixed points, which is calculated to one-loop order, too. Thus no further approximations are necessary to be consistent.

Very close to the critical temperature T_I an ε-expansion or Borel resummation[36] would of course be inevitable in order to obtain better values for the critical exponents. A description of the generalized minimal subtraction scheme is for example given in Refs. 35,15,16 and 37. A crossover into an asymptotically Gaussian theory is described by this method in Ref. 17.

1. Flow equations

Our aim is to calculate the wavenumber and frequency dependence of the susceptibility to one-loop order. The field renormalization is zero to one loop order. Thus we will not take into account corrections to the static exponent η and corrections to the mean-field value of the

dynamic exponent $z \approx 2$. This leaves $r_\circ$ and $u_\circ$ as the only quantities to be renormalized.[17]

There is a shift of the critical temperature from the mean-field result $T_{\circ I}$ to the "true" transition temperature T_I. In order to take this shift into account, a transformation to a new temperature variable, being zero at the critical temperature T_I, is performed. This new variable will be denoted again as $\tau_\circ$. The only renormalized quantities are then written as

$$\tau = Z_r^{-1}\tau_\circ \mu^{-2} \tag{4.19}$$

$$u = Z_u^{-1} u_\circ A_d \mu^{-\varepsilon} \ . \tag{4.20}$$

Here, the geometric factor A_d is chosen[36] as

$$A_d = \frac{\Gamma(3-d/2)}{2^{d-2}\pi^{d/2}(d-2)} \ . \tag{4.21}$$

For the non-trivial Z factors one finds in the generalized minimal subtraction procedure (see App. A)

$$Z_u = 1 + \frac{n+8}{6\varepsilon} u_\circ A_d \mu^{-\varepsilon} \frac{1}{(1+\tau_\circ/\mu^2)^{\varepsilon/2}} \ , \tag{4.22}$$

$$Z_r = 1 + \frac{n+2}{6\varepsilon} u_\circ A_d \mu^{-\varepsilon} \frac{1}{(1+\tau_\circ/\mu^2)^{\varepsilon/2}} \ . \tag{4.23}$$

Setting $\tau_\circ = 0$ the familiar renormalization constants for the n-component ϕ^4 model are recovered. In general here, however, the Z factors are functions of both $u_\circ$ and $\tau_\circ$.[35] In the next step the fact that the unrenormalized N-point functions do not depend on the scale μ is exploited and the Callan-Symanzik equations are derived.[26] The idea behind that is to connect via the renormalization-group equations the uncritical theory, which can be treated perturbationally, with the critical theory displaying infrared divergences. The resulting partial differential equations can be solved with the method of characteristics ($\mu(l) = \mu\, l$). With the definition of Wilson's flow functions

$$\zeta_\tau(l) = \mu \frac{\partial}{\partial \mu}\bigg|_0 \ln \frac{\tau}{\tau_\circ} \ , \tag{4.24}$$

$$\beta_u(l) = \mu \frac{\partial}{\partial \mu}\bigg|_0 u \ , \tag{4.25}$$

we proceed to the flow dependent couplings $\tau(l)$ and $u(l)$ (see Eqs. 4.19 and 4.20)

$$l\frac{\partial \tau(l)}{\partial l} = \tau(l)\zeta_\tau(l) \ , \tag{4.26}$$

$$l\frac{\partial u(l)}{\partial l} = \beta_u(l) \tag{4.27}$$

given by the first order ordinary differential equations

$$l\,\frac{\partial \tau(l)}{\partial l} = \tau(l)\left(-2 + \frac{n+2}{6}u(l)\frac{1}{[1+\tau(l)]^{1+\varepsilon/2}}\right) \ , \tag{4.28}$$

$$l\,\frac{\partial u(l)}{\partial l} = u(l)\left(-\varepsilon + \frac{n+8}{6}u(l)\frac{1}{[1+\tau(l)]^{1+\varepsilon/2}}\right) \ , \tag{4.29}$$

and the initial conditions $\tau(1) = \tau$ and $u(1) = u$. The asymptotic behavior is determined by zeros of the β function, giving the fixed points of the renormalization group. Here, we find the Gaussian fixed point $u_G^* = 0$ with $\zeta_G^* = -2$ and the Heisenberg fixed point $u_H^* = \frac{6\varepsilon}{n+8}$ with $\zeta_H^* = -2 + \varepsilon$. These fixed points are of course well-known,[26] but in the generalized minimal subtraction scheme it is now possible to describe the crossover between these two fixed points. We are interested in the theory in three dimensions and will henceforth discuss this case ($\varepsilon = 1$).

First we investigate the crossover of the $\tau(l)$ flow. It is possible to recover the universal crossover in the flow by plotting $\tau(l)$ against the scaling variable (compare Refs. 10,16,17)

$$x = \frac{l}{\tau(1)^{1/(2-\frac{n+2}{n+8})}} \ . \tag{4.30}$$

In Fig. 1 the effective exponent for the x-dependence of $\tau(l)$ is depicted for ten different values of $\tau(1)$ [with fixed $u(1)$ and $n = 2$], coinciding perfectly. There is a crossover from the region $l \to 0$ with the exponent -2 to the region $l \to 1$ with the exponent $-2 + (n+2)/(n+8)$.

Next we find, with the scaling variable $x \propto (k\xi)^{-1}$, the effective exponent ν_{eff} of the temperature dependence of the correlation length

$$\tau(l) \propto l^{-1/\nu_{\text{eff}}} \quad \Rightarrow \quad \frac{1}{\nu_{\text{eff}}} = \begin{cases} 2 & l \to 0 \\ 2 - \frac{n+2}{n+8} & l \approx 1 \end{cases} \tag{4.31}$$

Thus, with the generalized minimal-subtraction scheme we can describe the crossover from the non-classical critical behavior to the Gaussian behavior, e.g., as a function of the temperature variable τ.

2. Matching

To one-loop order, only the tadpole graph enters in the two-point function (see $\Gamma_{\circ\tilde{\psi}\psi}$ in App. A) shifting the critical temperature as stated above. Thus the susceptibility does not change its form and the renormalized version reads with Eq. (2.12), Eq. (2.15) and App. A to one-loop order,

$$\chi_R^{-1}(\mathbf{k},\omega) = k^2 - i\omega/\lambda + \tau(l)\mu^2 l^2 \ . \tag{4.32}$$

Yet what we gained in the last subsection was the temperature dependence of the coupling constants. We have to take into consideration this temperature dependence in order to discuss the changes resulting from the fluctuation corrections. One now has to ask the question: how

does the flow enter the physical quantities measured in an experiment?

With the flow dependence of the coupling constants, the relaxation rate to one-loop order becomes [see Eq. (3.3)]

$$\begin{aligned}\frac{1}{T_1} &\propto \int k^2 dk \frac{\Im\chi_R(\mathbf{k},\omega_L)}{\omega_L} \\ &= \int k^2 dk \frac{1}{\omega_L^2/\lambda^2 + [k^2+\tau(l)\mu^2 l^2]^2} \cdot \frac{1}{\lambda} \\ &= \frac{1}{\mu l}\frac{1}{\lambda}\int \tilde{k}^2 d\tilde{k} \frac{1}{\tilde{\omega}_L^2 + [\tilde{k}^2+\tau(l)]^2} \end{aligned} \tag{4.33}$$

where $\tilde{k} = k/\mu l$ and $\tilde{\omega}_L = \omega_L/\lambda\mu^2 l^2$.

Keeping $r(l)$ fixed (it is set to 1) the relaxation rate $1/T_1$ is proportional to l^{-1} for large l. When l approaches zero a constant value of the integral and hence of the relaxation rate $1/T_1$ will be reached, because of the fixed time scale $1/\tilde{\omega}_L$. The physical reason is that in the slow motion limit the characteristic time scale $(1/\omega_\varphi)$ becomes larger than the experimental time scale $1/\tilde{\omega}_L$. In Fig. 2 the logarithmic l dependence of the integral

$$I_1 \equiv \frac{\partial \log T_1}{\partial \log l} = -\frac{\partial \log\left(\frac{1}{\mu l\lambda}\int \tilde{k}^2 d\tilde{k}\frac{1}{\tilde{\omega}_L^2 + (\tilde{k}^2+1)^2}\right)}{\partial \log l} \tag{4.34}$$

is plotted against the scaling variable

$$x = l \cdot \frac{\mu\sqrt{\lambda}}{\sqrt{\omega_L}} \,. \tag{4.35}$$

We regain the transition from the l-independent regime ($l \to 0$) (and therefore of the temperature-independent regime) to the regime $I_1 \propto l$ ($l \to \infty$). This corresponds to the transition from the slow-motion to the fast-motion limit; a change of l is aquivalent to a change of ω_φ.

However, we are rather interested in the dependence of the relaxation rate from the physical temperature $\tau(1)$ than from the flow parameter l. This may be obtained as follows. Knowing the solution of the flow equations $\tau(l)$ and $u(l)$, we can find a l_1 for a given $\tau(1)$ that fulfills the equation $\tau(l_1) = 1$. Inverting this relation, $\tau(1)$ for a given l_1 with $\tau(l_1) = 1$ can be found. It is not possible to write down an analytical expression, but numerically this relationship is readily obtained. Thus we are led to $1/T_1(r(1)) = 1/T_1(l_1[r(1)])$. To connect the theory in a region where the perturbation expansion is valid with the interesting region, we match the temperature variable $r(l)$ to 1, thus imposing the crossover behavior of the flow $r(l)$ to the effective exponent of the relaxation time $1/T_1$.

In Fig. 3 the resulting $T_1(T)$ dependence is used to fit experimental NMR data for Rb_2ZnCl_4 (measured points are indicated by circles) from Mischo et al.[38] Two parameters have to be fixed in the theory. First, the prefactor relating the relaxation rate and the integral over the imaginary part of the susceptibility in Eq. (4.33) must be determined. Thus, the value of $1/T_1(T = T_I)$ is set. The second parameter is the scale of ω_L compared to the coupling $\lambda\mu$. With this the relative temperature ΔT, where the transition between slow and fast motion limit takes place, is adjusted.

The two fit curves presented in Fig. 3 show a crossover to the mean-field regime starting at $\Delta T \approx 10K$ (a) and at $\Delta T \approx 5K$ (b). A very good agreement, not only for the transition from the slow to the fast motion limit, but also for the high-temperature behavior is found in the second case. We want to discuss this issue now in more detail.

3. Width of the Critical Region

Some experiments report large regions in which non-classical exponents for the temperature dependence of the relaxation rate are observed. E.g., in Ref. 20 the range above T_I where non-classical exponents are found is $\Delta T \approx 100K$. These findings have to be understood by means of the Ginzburg-Levanyuk[39,40] argument, which states that only near to the critical temperature the non-classical critical exponents should be valid. Fluctuations should contribute only near the critical point and change the mean-field picture there.

The property of the integral quantity $1/T_1$, in the region where a crossover between the non-classical critical exponents and the mean-field exponents occurs, was studied in the last subsection. We now comment on the four regions that can be identified and are indicated by numbers $1 \ldots 4$ in Fig. 4.

Very close to T_I, there is a temperature-independent region (1), because of the dominating scale ω_L. Here, the probing frequency ω_L is too fast to grasp the critical behavior. Upon going to higher temperatures, after a transition region (2), a temperature dependence with non-classical critical exponents emerges (3). For even higher temperatures one finds a crossover to the mean-field exponents, in regime (4). In Fig. 4 this crossover takes place between $\Delta T \approx 5K$ and $\Delta T \approx 20K$. From Fig. 3, we find that the crossover at lower temperatures, here starting at $\Delta T \approx 5K$, leads to a better fit of the experimental data. Thus the reported large region, where supposedly non-classical exponents are found,[20] is in our opinion not an indispensable conclusion that can be drawn from the experimental data. The plausible scenario of an extended crossover regime beyond the truly asymptotic region of width $\Delta T \approx 5K$ is in fact in perfect agreement with the data.

As this is not a universal feature other scenarios are possible. It may happen that the scale of ω_L is very large and thus only the Gaussian exponents are found. We omitted the contribution of higher Raman processes, as discussed by Holzer et al.,[20] leading to an additional T^2 dependence for the relaxation rate. These would bend

the curves downward even more and explain the deviation present at the highest measured temperatures. Not taking these additional contributions into consideration, however, clarifies the crossover aspect.

V. LOW-TEMPERATURE PHASE

This section is devoted to the incommensurate ordered phase below the critical temperature T_I. In the $O(n)$-symmetrical model a spontaneous breaking of a global continuous symmetry occurs and the expectation value of the order parameter becomes nonzero. Now parallel and perpendicular fluctuations with respect to the nonzero order parameter have to be distinguished. As a consequence there appear $n-1$ massless Goldstone modes which lead to infrared singularities for all temperatures below T_I in certain correlation functions.[7,8] We investigate how these Goldstone modes influence the dynamical properties of the quantities we are interested in, e.g., the NMR relaxation rate. To do so, we first derive the dynamical functional appropriate below T_I. In the following subsection some comments about the Goldstone anomalies are made. We will then treat the dynamics of the fluctuations parallel (amplitudons) and perpendicular (phasons) to the order parameter. Again a renormalization group calculation to one-loop order is presented. We will discuss the dynamical susceptibility before evaluating the integrals leading to the relaxation rate. In the last section, we compare with experimental data. We also comment on the existence of a phason gap.

A. Dynamical functional

Let us assume that the spontaneous symmetry breaking below T_I appears in the nth direction of the order parameter space. As usual, new fields $\pi_\circ^\alpha$, $\alpha = 1, \ldots, n-1$, and $\sigma_\circ$ are introduced[15]

$$\begin{pmatrix} \tilde{\psi}_\circ^\alpha \\ \tilde{\psi}_\circ^n \end{pmatrix} = \begin{pmatrix} \tilde{\pi}_\circ^\alpha \\ \tilde{\sigma}_\circ \end{pmatrix} \quad , \qquad \begin{pmatrix} \psi_\circ^\alpha \\ \psi_\circ^n \end{pmatrix} = \begin{pmatrix} \pi_\circ^\alpha \\ \sigma_\circ + \bar{\phi}_\circ \end{pmatrix} \quad , \tag{5.1}$$

with

$$\langle \pi_\circ^\alpha \rangle = \langle \sigma_\circ \rangle = 0 \; . \tag{5.2}$$

The order parameter is parameterized as

$$\bar{\phi}_\circ = \sqrt{\frac{3}{u_\circ}}\, m_\circ \; . \tag{5.3}$$

Thus $\sigma_\circ$ corresponds to the longitudinal, and $\pi_\circ^\alpha$ to the transverse fluctuations.

Inserting these transformations into the functional (2.10) leads to a new functional of the form $J = J_0 + J_{int} + J_1 + const$ with[16]

$$\begin{aligned} J_0[\{\tilde{\pi}_\circ^\alpha\}, \tilde{\sigma}_\circ, \{\pi_\circ^\alpha\}, \sigma_\circ] = \\ \int_k \int_\omega \Big[\sum_\alpha \lambda_\circ \; \tilde{\pi}_\circ^\alpha(\mathbf{k},\omega)\, \tilde{\pi}_\circ^\alpha(-\mathbf{k},-\omega) \\ + \lambda_\circ \, \tilde{\sigma}_\circ(\mathbf{k},\omega)\, \tilde{\sigma}_\circ(-\mathbf{k},-\omega) \\ - \sum_\alpha \tilde{\pi}_\circ^\alpha(\mathbf{k},\omega) \left[i\omega + \lambda_\circ \left(r_\circ + \frac{m_\circ^2}{2} + k^2 \right) \right] \pi_\circ^\alpha(-\mathbf{k},-\omega) \\ - \tilde{\sigma}_\circ(\mathbf{k},\omega) \left[i\omega + \lambda_\circ \left(r_\circ + \frac{3\, m_\circ^2}{2} + k^2 \right) \right] \sigma_\circ(-\mathbf{k},-\omega) \Big] \; , \end{aligned} \tag{5.4}$$

$$\begin{aligned} J_{int}[\{\tilde{\pi}_\circ^\alpha\}, \tilde{\sigma}_\circ, \{\pi_\circ^\alpha\}, \sigma_\circ] = \\ - \frac{1}{6}\, \lambda_\circ \, u_\circ \int_{k_1 k_2 k_3 k_4} \int_{\omega_1 \omega_2 \omega_3 \omega_4} \delta\Big(\sum_i \mathbf{k}_i \Big) \; \delta\Big(\sum_i \omega_i \Big) \\ \times \Big[\sum_{\alpha\beta} \tilde{\pi}_\circ^\alpha(\mathbf{k}_1,\omega_1)\, \pi_\circ^\alpha(\mathbf{k}_2,\omega_2)\, \pi_\circ^\beta(\mathbf{k}_3,\omega_3)\, \pi_\circ^\beta(\mathbf{k}_4,\omega_4) \\ + \sum_\alpha \tilde{\pi}_\circ^\alpha(\mathbf{k}_1,\omega_1)\, \pi_\circ^\alpha(\mathbf{k}_2,\omega_2)\, \sigma_\circ(\mathbf{k}_3,\omega_3)\, \sigma_\circ(\mathbf{k}_4,\omega_4) \\ + \sum_\alpha \tilde{\sigma}_\circ(\mathbf{k}_1,\omega_1)\, \pi_\circ^\alpha(\mathbf{k}_2,\omega_2)\, \pi_\circ^\alpha(\mathbf{k}_3,\omega_3)\, \sigma_\circ(\mathbf{k}_4,\omega_4) \\ + \tilde{\sigma}_\circ(\mathbf{k}_1,\omega_1)\, \sigma_\circ(\mathbf{k}_2,\omega_2)\, \sigma_\circ(\mathbf{k}_3,\omega_3)\, \sigma_\circ(\mathbf{k}_4,\omega_4) \Big] \\ - \lambda_\circ \sqrt{\frac{3\, u_\circ}{6}}\, m_\circ \int_{k_1 k_2 k_3} \int_{\omega_1 \omega_2 \omega_3} \delta\Big(\sum_i \mathbf{k}_i \Big) \; \delta\Big(\sum_i \omega_i \Big) \\ \times \Big[\sum_\alpha 2\, \tilde{\pi}_\circ^\alpha(\mathbf{k}_1,\omega_1)\, \pi_\circ^\alpha(\mathbf{k}_2,\omega_2)\, \sigma_\circ(\mathbf{k}_3,\omega_3) \\ + \sum_\alpha \tilde{\sigma}_\circ(\mathbf{k}_1,\omega_1)\, \pi_\circ^\alpha(\mathbf{k}_2,\omega_2)\, \pi_\circ^\alpha(\mathbf{k}_3,\omega_3) \\ + 3\, \tilde{\sigma}_\circ(\mathbf{k}_1,\omega_1)\, \sigma_\circ(\mathbf{k}_2,\omega_2)\, \sigma_\circ(\mathbf{k}_3,\omega_3) \Big] \; , \end{aligned} \tag{5.5}$$

and

$$\begin{aligned} J_1[\tilde{\sigma}_\circ] = - \lambda_\circ \sqrt{\frac{3}{u_\circ}}\, m_\circ \left(r_\circ + \frac{m_\circ^2}{2} \right) \\ \times \int_k \int_\omega \tilde{\sigma}_\circ(-\mathbf{k},-\omega) \delta(\mathbf{k},\omega) \; . \end{aligned} \tag{5.6}$$

Equation (5.2) ($\langle \sigma_\circ \rangle = 0$) yields a perturbative identity that gives the relation between $r_\circ$ and $m_\circ$, reading to one-loop order[15]

$$\begin{aligned} r_\circ + \frac{m_\circ^2}{2} = - \frac{n-1}{6}\, u_\circ \int_k \frac{1}{r_\circ + \frac{m_0^2}{2} + k^2} \\ - \frac{1}{2}\, u_\circ \int_k \frac{1}{r_\circ + \frac{3\, m_0^2}{2} + k^2} \; . \end{aligned} \tag{5.7}$$

In the following $r_\circ$ is replaced by $m_\circ$. Notice that by using the variable $m_\circ$, the shift of T_I is already incorporated [see Eq. (5.3)]. We can now write down the basic

ingredients needed to apply the recipe for the dynamical perturbation theory below T_I. The emerging propagators, vertices, and counterterms are listed with their graphical representation in Figs. 5, 6 and 7 (see Ref. 16).

B. Goldstone theorem and coexistence limit

As mentioned before, the particularity of the $O(n)$-symmetric functionals below the critical temperature is the occurrence of Goldstone modes in the entire low temperature phase.[5–7] Because no free energy is required for an infinitesimal quasistatic rotation of the order parameter, the transverse correlation length diverges in the limit of zero external field. The corresponding massless modes are the Goldstone modes,[5] in this context called phasons. They are manifest in non-analytical behavior of correlation functions, for example the longitudinal static susceptibility diverges and changes its leading behavior from being proportional to k^{-2} to[7,8,15,16]

$$\chi_L^{-1}(\mathbf{k},0) \propto k^{\varepsilon} \ . \tag{5.8}$$

Before discussing the details of the renormalization theory below T_I, we summarize some important aspects, which explain why below T_I an ε-expansion can be avoided. For more details see Ref. 16.

Leaving the critical temperature region $T \approx T_I$, which is characterized in the non-perturbed case by $m_\circ = 0$, and lowering the temperature, means that the fluctuations of the longitudinal modes (amplitudons) become negligible, because these modes are massive ($m_\circ$). In contrast the phasons remain massless and hence their fluctuations will dominate.

Yet a different way of describing the dominance of the fluctuations of the Goldstone modes is to consider the spherical model limit[8] $n \to \infty$. In this case of "maximal" symmetry breaking, the Goldstone modes are weighted with the factor $n-1 \to \infty$.

As mentioned above, below T_I coexistence anomalies are present. They arise from the fact that the $n-1$ transverse modes are massless. In the limit $k \to 0$ and $\omega \to 0$ for $T < T_I$ this manifests itself in typical infrared divergences. An important point to remember is that in order to gain these coexistence anomalies, one can also study the case $m_\circ \to \infty$. In the renormalization scheme it is shown that the flow of the mass parameter $m_\circ$ tends to infinity as the momentum and frequency tend to zero.

From this it is plausible, and was also proved[15], that in the coexistence limit the result for the two-point vertex functions are identical with the results arising from the spherical model limit $n \to \infty$.

These findings render an ε expansion unnecessary in the coexistence limit ($k \to 0$, $\omega \to 0$ at $m_\circ > 0$), because the asymptotic theory (the spherical model) is exactly treatable and reduces to the zero- and one-loop contributions. Of course, one has to make sure that the properties of the asymptotic functional will be reproduced in the respective limit. Within the generalized minimal subtraction scheme this is possible. As stated in subsection IV B Lawrie's method[15] and its dynamical extension in Ref. 16 lead beyond these limits and allow for a detailed study of the crossover behavior.

The behavior of the correlation functions in our case is driven by the crossover between the three fixed points present below T_I. Besides the Gaussian fixed point one finds the Heisenberg fixed point

$$[u_H = 6\epsilon/(n+8)] \tag{5.9}$$

and the coexistence fixed point[15]

$$[u_C = 6\epsilon/(n-1)] \ . \tag{5.10}$$

We will again employ the generalized minimal subtraction scheme to study the crossover between these fixed points.

C. Renormalization group analysis below T_I

1. Flow equations

Below T_I, using only the one-loop diagrams, again the field renormalization vanishes. Hence, the only nontrivial Z factors are the ones for the temperature scale and the coupling constant:

$$m^2 = Z_m^{-1} m_\circ^2 \mu^{-2} \ , \tag{5.11}$$

$$u = Z_u^{-1} u_\circ A_d \mu^{-\varepsilon} \ . \tag{5.12}$$

Because we use m instead of r an important relationship can be stated, which is true independently of the loop order,[16]

$$Z_m \cdot Z_\sigma = Z_u \ . \tag{5.13}$$

To one-loop order ($Z_\sigma = 1$) we find (see App. A)[16]

$$\begin{aligned} Z_u = Z_m =& 1 + \frac{n-1}{6\varepsilon} u_\circ A_d \mu^{-\varepsilon} \\ &+ \frac{3}{2\varepsilon} u_\circ A_d \mu^{-\varepsilon} \frac{1}{(1+m_\circ^2/\mu^2)^{\varepsilon/2}} \ . \end{aligned} \tag{5.14}$$

Here, the contribution of the transverse loops lead to different divergences manifest in the change of the Z factors compared to those above T_I [see Eq. (4.23)]. We recover the familiar renormalization constant in the critical region by setting $m_\circ = 0$. When considering the coexistence limit $m_\circ \to \infty$, the weight of the effective critical fluctuations is reduced from $n+8$ to $n-1$, the number of Goldstone modes.

Asymptotically ($m \to \infty$) the Z factors are exact. In the crossover region they are an approximation to the order $u_\circ^2/(1+m_\circ/\mu^2)^{\varepsilon/2}$.[16]

From this we directly derive the flow-dependent couplings

$$l\,\frac{\partial m(l)}{\partial l} = \frac{1}{2} m(l) \left(-2 + \frac{n-1}{6} u(l) + \frac{3}{2} \frac{u(l)}{[1+m(l)^2]^{1+\varepsilon/2}} \right) , \tag{5.15}$$

$$l\,\frac{\partial u(l)}{\partial l} = u(l) \left(-\varepsilon + \frac{n-1}{6} u(l) + \frac{3}{2} \frac{u(l)}{[1+m(l)^2]^{1+\varepsilon/2}} \right) . \tag{5.16}$$

Wilson's flow equations β_u and ζ_m now read

$$l \frac{\partial m(l)}{\partial l} = \frac{1}{2} m(l) \zeta_m(l) , \tag{5.17}$$

$$l \frac{\partial u(l)}{\partial l} = \beta_u(l) . \tag{5.18}$$

Three fixed points have now to be taken into consideration.[15,16] Next to the Gaussian fixed point $u_G^* = 0$ with $\zeta_{mG}^* = -2$, we find in the critical limit ($m_\circ \to 0$) the infrared-stable Heisenberg fixed point $u_H^* = 6\varepsilon/(n+8)$ with $\zeta_{mH}^* = -2+\varepsilon$. In the coexistence limit $m_\circ \to \infty$, we find in addition to the still ultraviolet-stable Gaussian fixed point the coexistence fixed point, identified by Lawrie,[15] $u_C^* = 6\varepsilon/(n-1)$ with $\zeta_{mH}^* = -2+\varepsilon$, which is infrared-stable. Thus $m(l)^2$ diverges asymptotically for $l \to 0$ as $l^{-2+\varepsilon}$, if $\varepsilon < 2$. Indeed, the coexistence limit is described by a divergent mass parameter.

In Figs. 8 and 9 the flow for $m(l)$ and $u(l)$ is plotted. We find for the flow $u(l)$ a crossover between the coexistence fixed point, inversely proportional to the number of Goldstone modes $(n-1)$, and the Heisenberg fixed point

$$u(l) \quad \Rightarrow \begin{cases} 6\varepsilon/(n-1) & l \to 0 \\ 6\varepsilon/(n+8) & l \approx 1 . \end{cases} \tag{5.19}$$

That means that for $m(1) \ll 1$ the coexistence limit is not approached directly for $l \to 0$, but for a while the flow stays near the Heisenberg fixed point regime. The scaling variable for $u(l)$ is here[10,16]

$$x = \frac{l}{m(1)^{2/(2-\varepsilon)}} , \tag{5.20}$$

again leading to perfectly coinciding curves when plotted vs. x.

From the relation stated in Eq. (5.13) one can deduce the renormalization-group invariant[16]

$$\frac{m(l)^2}{u(l)} l^{2-\varepsilon} = \frac{m(1)^2}{u(1)} , \tag{5.21}$$

which immediately gives us the scaling of $m(l)$ that can be observed in Fig. 8,

$$m(l)^2 \propto l^{-1/\nu_{\rm eff}} \quad \text{with} \quad \frac{1}{\nu_{\rm eff}} = \begin{cases} 2-\varepsilon & l \to 0 \\ 2 - \frac{n+2}{n+8} & l \approx 1 . \end{cases} \tag{5.22}$$

Notice that the value of $1/\nu_{\rm eff}$ in the first case is the same as $1/\nu$ for the spherical model. The mass parameter m diverges for $l \to 0$, $m(l)^2 \propto l^{-2+\varepsilon}$ with $\varepsilon < 2$.

From now on we will concentrate on three dimensions ($\varepsilon = 1$) and $n = 2$.

2. Matching

In order to discuss the static susceptibility we use the matching condition $\mu l = k$. This relation connects the dependence of the renormalized quantities on the momentum scale μ with the k dependence, in which we are interested.

For the integrated value, we are interested in the temperature dependence rather than the dependence on the flow parameter l or the wavevector k. Thus, after integration we have to again match the resulting l-dependent relaxation rate with the physical temperature (see section IV B).

D. Susceptibility

In order to determine the renormalized dynamical susceptibility, we evaluate the one-loop diagrams for the two-point cumulants, which can be easily derived from the one-loop vertex functions listed in Appendix A.[16] Below T_I, the structure of the susceptibility does change to one loop order, compared to the mean-field results. We write in a general form

$$\chi_{\circ\,\perp/\parallel}^{-1}(\mathbf{k},\omega) = \frac{-i\omega}{\lambda_\circ} + k^2 + f_\circ^{\perp/\parallel}(\mathbf{k},\omega) , \tag{5.23}$$

with the self-energy $f_\circ^{\perp/\parallel}$ containing the contributions of the one-loop diagrams. The explicit form of $f_\circ^{\perp/\parallel}$ is gained from the calculation of the two-point vertex function in App. A and Eqs. (2.12) and (2.15). We then obtain the renormalized susceptibility $\chi_{\parallel,\perp}^R$ by inserting the Z factors with the flow dependent coupling constants $u(l)$ and $m(l)$. Because no field renormalization is present, we can replace $\lambda_\circ$ with λ to this order. This is because via the fluctuation-dissipation theorem (2.13), Z_λ and the field renormalizations are connected.

1. Amplitudon modes

In $d = 3$ the longitudinal susceptibility characterizing the amplitudon modes is given by[16]

$$\chi_\parallel^R(\mathbf{k},\omega) = \frac{1}{k^2 - i\,\omega/\lambda + \mu^2\,l^2\,m(l)^2\,Z_m(l)}\left(1 + \frac{1}{(k^2 - i\,\omega/\lambda)/\mu^2\,l^2 + m(l)^2}\,\frac{u(l)\,m(l)^2}{2\,k/\mu\,l}\right.$$
$$\times\left[\frac{n-1}{3}\left(\frac{\pi}{2} + \arcsin\frac{i\,\omega/\lambda}{k^2 - i\,\omega/\lambda}\right) + 3\left(\arcsin\frac{i\,\omega/\lambda\,\mu^2\,l^2}{\left[\left([k^2 - i\,\omega/\lambda]/\mu^2\,l^2\right)^2 + 4\,m(l)^2\,k^2/\mu^2\,l^2\right]^{1/2}}\right.\right.$$
$$\left.\left.\left. + \arcsin\frac{(k^2 - i\,\omega/\lambda)/\mu^2\,l^2}{\left[\left([k^2 - i\,\omega/\lambda]/\mu^2\,l^2\right)^2 + 4\,m(l)^2\,k^2/\mu^2\,l^2\right]^{1/2}}\right)\right]\right) \tag{5.24}$$

First we want to discuss some limits in order to become acquainted with this complex form of the susceptibility.

It is important to notice the change of the structure of the RG susceptibility that results from the one-loop contribution of the perturbation theory. To clarify this, we state the asymptotic susceptibility, which is evaluated for non-zero frequency ($\mathbf{k} \to 0, \omega > 0$)

$$\chi_\parallel^R = \frac{1}{k^2 - i\omega/\lambda + m(1)^2 \cdot k \cdot \dfrac{1}{1 + a \cdot g(k)}} \tag{5.25}$$

with a constant a and a function $g(k)$ that is regular for $q \to 0$. From this limit, it becomes clear that we have to expect changes of the scaling behavior.

In the coexistence limit ($\omega = 0, \mathbf{k} \to 0$) we recover the exact asymptotic result ($d = 3$, $\varepsilon = 1$)

$$\chi_\parallel^R \propto k^{-1} \tag{5.26}$$

displaying the coexistence anomaly. When keeping the frequency $\omega > 0$ fixed ($\mathbf{k} \to 0, \omega \neq 0$) the imaginary part of the susceptibility approaches a constant value

$$\chi_\parallel^R \Rightarrow h(\omega)\ . \tag{5.27}$$

where $h(\omega)$ is a function of ω only. We can now turn to the full susceptibility. The imaginary part of the susceptibility is plotted for different temperatures in Fig. 10. The structure of $\Im\chi_\parallel^R$ changes dramatically as compared to the mean-field result, as to be expected. The contributions of the phason and amplitudon loops are given by the terms in brackets of Eq. (5.24). They give rise to a qualitatively different behavior of $\chi_\parallel^R$. Different scaling regions can be identified. Expanding the imaginary part of $\chi_\parallel^R$ yields analytical expressions for the scaling regions, as listed in Table II. While the $k \to \infty$ and $k \to 0$ behavior reproduces the mean-field result, the correct treatment of the Goldstone anomalies lead to an additional k^{-3} behavior in the intermediate region $\sqrt{\omega/\lambda} < k < m(1)$. A plateau appears for smaller k and temperatures far away from the critical temperature T_I. The effective exponent κ of the k dependence of $\Im\chi_\parallel^R$ is plotted in Fig. 11. One can therefrom easily identify the scaling regions presented in Table II.

The influence of the Goldstone modes is therefore to alter the k dependence of the susceptibility not only in the coexistence limit, but also in intermediate regions. In order to derive the temperature dependence of $\chi_\parallel^R$, in addition the flows of $m(l)$ and $u(l)$ need to be considered.

2. Phason modes

For the transverse susceptibility characterizing the phason modes one finds[16]

$$\chi_\perp^R(\mathbf{k},\omega) = \frac{1}{k^2 - i\,\omega/\lambda}\left(1 - \frac{u(l)\,m(l)/6}{(k^2 - i\,\omega/\lambda)/\mu^2\,l^2}\left[2 - \frac{m(l)}{k/\mu\,l}\left(\frac{\pi}{2} - \arcsin\frac{-i\,\omega/\lambda\,\mu^2 l^2 + m(l)^2}{(k^2 - i\,\omega/\lambda)/\mu^2\,l^2 + m(l)^2}\right.\right.\right.$$
$$+ \arcsin\frac{i\,\omega/\lambda\,\mu^2\,l^2 + m(l)^2}{\left[\left((k^2 - i\,\omega/\lambda)/\mu^2\,l^2 - m(l)^2\right)^2 + 4\,m(l)^2\,k^2/\mu^2\,l^2\right]^{1/2}}$$
$$\left.\left.\left. + \arcsin\frac{(k^2 - i\,\omega)/\lambda\mu^2\,l^2 - m(l)^2}{\left[\left((k^2 - i\,\omega/\lambda)/\mu^2\,l^2 - m(l)^2\right)^2 + 4\,m(l)^2\,k^2/\mu^2\,l^2\right]^{1/2}}\right)\right]\right)\ . \tag{5.28}$$

Here the problem lies in the cancellation of terms with respect to their k dependence, hidden in the complex structure of Eq. (5.28). Hence we start again with considering the coexistence limit ($\mathbf{k} \to 0, \omega \to 0$):

$$\chi_{\perp}^{R} \propto k^{-2} \; , \tag{5.29}$$

which is easily found. The results for $\mathbf{k} \to 0, \omega \neq 0$ are more difficult to obtain, because the arcsin-terms cancel their k-dependence against each other. In two limits this can be done analytically. For $m \to 0$ one gets

$$\chi_{\perp}^{R} \to \chi_{\circ\perp} = \frac{1}{k^2 - i\omega/\lambda} \tag{5.30}$$

reproducing the mean-field susceptibility for the massless transverse modes.

For $m \to \infty$ the arcsin-terms read as $\frac{2}{m} + c_1 \frac{1}{m^3} + c_2 \frac{i\omega}{\lambda k^2} \cdot \frac{1}{m^3}$ leading to

$$\chi_{\perp}^{R} \to \frac{1}{k^2 - i\omega/\lambda + \dfrac{1}{6} u(l)(c_1 k^2 + c_2 \frac{i\omega}{\lambda})/m(l)} \tag{5.31}$$

Here c_1 and c_2 are constants. Thus in the two extreme limits, the temperature dependence vanishes, and only in between, for $m(l) \propto \mathcal{O}(1)$ can we expect a slightly temperature-dependent behavior.

In Figs. 12 and 13 the imaginary part of the transverse susceptibility and its effective exponent with respect to k are plotted for different temperatures. Notice that leaving the critical temperature leads to a temperature dependence. This is caused by the coupling of the amplitudon and phason modes. Yet as the temperature is further reduced, the temperature dependence disappears again.

E. Relaxation rate

In this subsection we study consequences for the relaxation arising from the Goldstone anomalies present in the susceptibility. As mentioned in Sec. III, in order to gain the relaxation rate we have to integrate over the imaginary part of the susceptibility.

Because the transverse susceptibility is temperature dependent, also the relaxation rate, connected with the phasons, will be temperature dependent. This is of course not the case in the mean-field analysis. As discussed in the last section, for $T \to T_I$ the susceptibility approaches the mean-field result, and thus the relaxation rate at the critical temperature is unaltered.

For the relaxation rate connected with the amplitudons the changes are more subtle. Therefore, we collect all the contributions from the one-loop diagrams in a function $f(\mathbf{k}, \omega)$, which can be interpreted as a $\mathbf{k}$- and ω-dependent dimensionless self-energy. The susceptibility has now the following structure

$$(\chi_{\parallel}^{R})^{-1} = k^2 - i\omega/\lambda + f(\mathbf{k}, \omega)\mu^2 l^2 \tag{5.32}$$

The dependence of f on k and ω is plotted in Fig. 14. We see that the real part of the effective mass f is decreasing for $k \to 0$. Thus, the Goldstone anomalies lead to a reduction of the real part of f. In the coexistence limit, $\omega \to 0$ and small k, the real part of f tends to 0 linearly and relation (5.26) is recovered. The imaginary part is only k-dependent for very small k. That means, when we integrate over all k the influence of the Goldstone anomalies can be interpreted as follows. The effective Larmor frequency is raised and the mass is lowered for small k as compared to the mean-field description. We can easily derive this easily from the longitudinal relaxation rate with $f(k, \omega)$ taken into consideration

$$\begin{aligned}
\frac{1}{T_1^{\parallel}} &\propto \int k^2 dk \frac{\Im \chi_{\parallel}^{R}(\mathbf{k}, \omega_L)}{\omega_L} \\
&= \int k^2 dk \frac{1}{\mu^2 l^2 \omega_L} \\
&\quad \times \frac{\tilde{\omega} - \Im f^{\parallel}(\tilde{\mathbf{k}}, \tilde{\omega})}{[\tilde{\omega}^2 - \Im f^{\parallel}(\tilde{\mathbf{k}}, \tilde{\omega})]^2 + [\tilde{k}^2 + \Re f^{\parallel}(\tilde{\mathbf{k}}, \tilde{\omega})]^2} \\
&= \frac{1}{\mu l} \frac{1}{\lambda} \int \tilde{k}^2 d\tilde{k} \\
&\quad \times \frac{1 - \Im f^{\parallel}(\tilde{\mathbf{k}}, \tilde{\omega})/\tilde{\omega}}{[\tilde{\omega} - \Im f^{\parallel}(\tilde{\mathbf{k}}, \tilde{\omega})]^2 + [\tilde{k}^2 + \Re f^{\parallel}(\tilde{\mathbf{k}}, \tilde{\omega})]^2} \; ,
\end{aligned} \tag{5.33}$$

where again $\tilde{k} = k/\mu l$ and $\tilde{\omega} = \omega_L/\lambda \mu^2 l^2$. When we compare this result to the mean-field result, the interpretation given above becomes clear. The relaxation rate is raised through the influence of the Goldstone modes. Both the transverse and longitudinal relaxation times are plotted in Fig. 15. Again we have compared our findings with experimental data, taken from Ref. 38. In the low-temperature phase we have less freedom of choice in our theory, as the scale $T_1(T = T_I)$ and the parameters are already fixed by their high-temperature values. Thus only one parameter is left to be adjusted.

In the vicinity of T_I we find a temperature-independent region, because both the transverse and the longitudinal susceptibility become temperature-independent and approach their mean-field values.

The transverse relaxation time shows a slight temperature dependence for temperatures further away from T_I. If we use the identical choice of parameters as for the high-temperature phase, we find good agreement in the low-temperature phase as well. The temperature where the maximum value of the transverse relaxation time in our theory is reached is identified with the corresponding temperature in the experiment. This temperature dependence is due to the coupling between the phason and amplitudon modes. We want to emphasize that, in agreement with the analysis of ultrasonic attenuation experiments,[9,10] no phason gap has to be introduced to explain the experimental data for Rb_2ZnCl_4. However,

it is important to treat the influence of the Goldstone modes beyond the mean-field approach.

For the longitudinal relaxation time, the crossover temperature represents additional an important scale. We used the same range $\Delta T \approx 5K$ as in the high-temperature phase for the plot in Fig. 15. Again good agreement between experiment and theory is observed. Both theory and experiment show two scaling regions, one above $\Delta T \approx 5K$ and one below. The qualitative behavior is correctly reproduced, but the quantitative agreement for the longitudinal relaxation rate is not as good as compared to the high-temperature phase. A possible reason may be the following. We calculated the coupling of the transverse and longitudinal order parameter fields to one-loop order. Below T_I, the coupling of the order parameter is changing the susceptibility in its structure, whereas above T_I nothing dramatic happens. One has to expect that below T_I this is of course only the first step beyond mean-field theory and the two-loop corrections might lead to quantitative modifications in the crossover region. Comparing the calculated transverse and the longitudinal relaxation rates below T_I with the experimental data is in agreement with this. A slight temperature dependence is not as sensitive as the scaling behavior of the longitudinal relaxation time, which has again two regimes due to the crossover scenario.

As the characteristic features are reproduced correctly, we may say that we understand the complex temperature dependence below T_I in the context of the coupled order parameter modes and a careful treatment of the Goldstone modes. Upon introducing the k- and ω-dependent self energy f we could in addition provide a physical interpretation of the changes of the longitudinal relaxation time, as compared to the mean-field analysis.

VI. CONCLUSIONS

In this paper we have presented a comprehensive description of the critical dynamics at structurally incommensurate phase transitions. Our starting point was the time-dependent, relaxational Ginzburg-Landau model with $O(2)$ symmetry. To be more general, we discussed the $O(n)$-symmetric functional. Hence, we were able to study the influence of the $n-1$ Goldstone modes accurately. We used the renormalization group theory in order to compute the dynamical susceptibility below and above the critical temperature T_I to one-loop order. Thus we could venture beyond the usual mean-field description. As we calculated the renormalization factors in the generalized minimal subtraction scheme,[35,15] we could deal with the interesting crossover scenarios carefully.[16]

Our findings were used to interpret experimental data from NMR experiments, measuring the relaxation rate. The relaxation rate is connected with the calculated susceptibility via an integral over the wavevector, at fixed frequency.

Above the critical temperature T_I, we showed how scaling arguments lead to an identification of the dynamical critical exponent for the relaxation rate and provide a qualitative understanding of its temperature dependence. Then we described the crossover from the critical region to a high-temperature region, where fluctuations should not change the classical critical exponents. Excellent agreement for both the critical exponents resulting from the scaling arguments and the description of the crossover regions with the experimental data was found. This led us to the conclusion that the experimental data should probably not be interpreted by identifying a critical region of supposed width of $100K$, but rather through a crossover between the non-classical critical exponents and the mean-field exponents, taking place at a temperature approximately equal to $T_I + 5K$. This conjecture yields a considerably more reasonable width of the critical region.

Below the critical temperature, we analyzed the dynamical susceptibility calculated to one-loop order in the renormalization group theory in considerable detail. The coupling of the OP modes was considered explicitly. We thus gained new insight into the influence of Goldstone modes on the structure of the susceptibility and its temperature dependence. As a result we found that the relaxation rate of the phason fluctuations becomes temperature-dependent. This temperature dependence disappears in the two limits when either the temperature approaches the critical temperature T_I, or the temperature is very low. For the amplitudon modes the influence of the Goldstone modes is more subtle. We summarized the effect in a wavevector- and frequency-dependent "mass" and showed that this can be interpreted as a bending-down of the temperature-dependent relaxation time as compared to a hypothetic situation where no Goldstone modes are present. All experimental findings are well understood treating the OP modes beyond their mean-field description. As reported from the analysis of ultrasonic attenuation experiments for Rb_2ZnCl_4 before,[9,10] no phason gap had to be introduced. Recently however, the direct observation of a "phason gap" has been reported for a molecular compound (BCPS).[41] This "phason gap" was observed in inelastic neutron scattering experiments for very high frequencies. Again, the low frequency dynamics probed by NMR did not reveal any gap.[42]

Thus, an interesting application of the $O(2)$-symmetric model is presented here, in terms of a crossover description and a discussion of the full k and ω dependence of the susceptibility calculated to one-loop order. We found very good agreement with experimental data. Besides the precise calculation of critical exponents as one strength of the renormalization group theory, also detailed analysis of crossover scenarios and the effect of the anharmonic coupling of modes is possible. We want to stress how successfully the results of the renormalization group theory can be applied to specific experimental find-

ings. In addition, we emphasize that the choice of two fit parameters in the phase above T_I already essentially determined the curves in the incommensurate phase.

The theory presented here is formulated in a general way. Therefore it could be readily used to analyze further experiments, especially below and near T_I.

ACKNOWLEDGMENTS

We benefited from discussions with E. Frey, J. Petersson, and D. Michel. B.A.K. and F.S. acknowledge support from the Deutsche Forschungsgemeinschaft under contract No. Schw. 348/6-1,2. U.C.T. acknowledges support also from the Deutsche Forschungsgemeinschaft through a habilitation fellowship DFG-Gz. Ta 177 / 2-1,2.

APPENDIX A:

In this appendix we list analytical results for the two-point vertex functions and their singularities ($1/\varepsilon$ poles) in the generalized minimal subtraction scheme, following from the dynamical functional (2.9). Below T_I, the corresponding zero- and one-loop contributions are stated. For the explicit calculation of the integrals in the generalized minimal subtraction scheme we refer to Ref. 43. All integrations over internal frequencies have already been performed by means of the residue theorem. We restrict ourselves to the three-dimensional case ($\varepsilon = 1$).

$\underline{T > T_I}$:
Here only the simplest one-loop graphs enter the diagrammatic expansion.

$$\begin{aligned}\Gamma_{\circ\tilde{\psi}\psi}(\mathbf{k},\omega) =&\lambda_\circ\left(k^2 + i\omega/\lambda_\circ + \tau_\circ + \frac{n+2}{6}u_\circ\int_q \frac{1}{\tau_\circ + q^2}\right)\\ =&\lambda_\circ\left(k^2 + i\omega/\lambda_\circ + \tau_\circ\left[1 - \frac{n+2}{6\varepsilon}u_\circ A_d\mu^{-\varepsilon}\frac{\tau_\circ}{(1+\tau_\circ/\mu^2)^{\varepsilon/2}}\right]\right)\\ =&\lambda_\circ\left(k^2 + i\omega/\lambda_\circ + \tau_\circ/Z_r\right)\end{aligned} \tag{A1}$$

$$\begin{aligned}\Gamma_{\circ\tilde{\psi}\psi\psi\psi}(\mathbf{k}_i = 0, \omega = 0) =&u_\circ - \frac{n+8}{6}u_\circ\int_q \frac{1}{(\tau_\circ + q^2)^2}\\ =&u_\circ\left[1 - \frac{n+8}{6\varepsilon}u_\circ A_d\mu^{-\varepsilon}\frac{1}{(1+\tau_\circ/\mu^2)^{\varepsilon/2}}\right]\\ =&u_\circ/Z_u\end{aligned} \tag{A2}$$

$\underline{T < T_I}$:
The diagrammatic expressions for the vertex functions are depicted in Figs. 16 and 17.

$$\begin{aligned}\Gamma_{\circ\ \tilde{\pi}\pi}(\mathbf{k},\omega) =&i\omega + \lambda_\circ\left(k^2 + \frac{1}{3}u_\circ m_\circ^2\int_q \frac{1}{q^2(m_\circ^2+q^2)}\right)\\ &- \lambda_\circ\frac{1}{3}u_\circ m_\circ^2\int_q \frac{1}{(\frac{\mathbf{k}}{2}-\mathbf{q})^2 + m_\circ^2}\cdot\frac{1}{i\omega/\lambda_\circ + (\frac{\mathbf{k}}{2}+\mathbf{q})^2 + m_\circ^2 + (\frac{\mathbf{k}}{2}-\mathbf{q})^2}\\ &- \lambda_\circ\frac{1}{3}u_\circ m_\circ^2\int_q \frac{1}{(\frac{\mathbf{k}}{2}-\mathbf{q})^2}\cdot\frac{1}{i\omega/\lambda_\circ + (\frac{\mathbf{k}}{2}+\mathbf{q})^2 + m_\circ^2 + (\frac{\mathbf{k}}{2}-\mathbf{q})^2}\\ =&i\omega + \lambda_\circ\left(k^2 + \frac{1}{3}u_\circ A_d m_\circ\right)\\ &+ \lambda_\circ\frac{1}{3}u_\circ m_\circ^2\cdot\frac{A_d}{2}\cdot\frac{1}{k}\left(\arcsin\frac{-i\omega/\lambda_\circ + m_\circ^2}{\sqrt{4m_\circ^2k^2 + (k^2 + i\omega/\lambda_\circ - m_\circ^2)^2}}\right.\\ &\left.+ \arcsin\frac{k^2 + i\omega/\lambda_\circ - m_\circ^2}{\sqrt{4m_\circ^2k^2 + (k^2 + i\omega/\lambda_\circ - m_\circ^2)^2}}\right)\\ &+ \lambda_\circ\frac{1}{3}u_\circ m_\circ^2\cdot\frac{A_d}{2}\cdot\frac{1}{k}\left(\frac{\pi}{2} - \arcsin\frac{i\omega/\lambda_\circ + m_\circ^2}{k^2 + i\omega/\lambda_\circ^2 + m_\circ^2}\right)\end{aligned} \tag{A3}$$

$$
\begin{aligned}
\Gamma_{\circ\ \tilde{\sigma}\sigma}(\mathbf{k},\omega) =& i\omega + \lambda_\circ \left(k^2 + m_\circ^2\right) \\
& - \lambda_\circ \frac{n-1}{3} u_\circ m_\circ^2 \int_q \frac{1}{(\frac{\mathbf{k}}{2}-\mathbf{q})^2 + m_\circ^2} \cdot \frac{1}{i\omega/\lambda_\circ + (\frac{\mathbf{k}}{2}+\mathbf{q})^2 + (\frac{\mathbf{k}}{2}-\mathbf{q})^2} \\
& - \lambda_\circ 3 u_\circ m_\circ^2 \int_q \frac{1}{(\frac{\mathbf{k}}{2}-\mathbf{q})^2 + m_\circ^2} \cdot \frac{1}{i\omega/\lambda_\circ + m_\circ^2 + (\frac{\mathbf{k}}{2}+\mathbf{q})^2 + m_\circ^2 + (\frac{\mathbf{k}}{2}-\mathbf{q})^2} \\
=& i\omega + \lambda_\circ \left(k^2 + m_\circ^2\right) \\
& + \lambda_\circ \frac{n-1}{3} u_\circ m_\circ^2 \cdot \frac{A_d}{2} \cdot \frac{1}{k} \left(\frac{\pi}{2} + \arcsin \frac{-i\omega/\lambda_\circ}{k^2 + i\omega/\lambda_\circ} \right) \\
& + \lambda_\circ 3 u_\circ m_\circ^2 \cdot \frac{A_d}{2} \cdot \frac{1}{k} \left(\arcsin \frac{-i\omega/\lambda_\circ}{\sqrt{4m_\circ^2 k^2 + (k^2 + i\omega/\lambda_\circ)^2}} \right. \\
& \left. + \arcsin \frac{k^2 + i\omega/\lambda_\circ}{\sqrt{4m_\circ^2 k^2 + (k^2 + i\omega/\lambda_\circ)^2}} \right)
\end{aligned}
\tag{A4}
$$

[1] W. Selke, in: *Phase Transitions and Critical Phenomena*, edited by C. Domb and J. L. Lebowitz (Academic Press, London, 1992) Vol. 15.
[2] R. Cowley and A. Bruce, J. Phys. C **11**, 3577 (1978).
[3] H. Z. Cummins, Phys. Rep. **185**, 211 (1990).
[4] A. Bruce and R. Cowley, J. Phys. C **11**, 3609 (1978).
[5] J. Goldstone, Nuovo Cimento **19**, 154 (1961).
[6] H. Wagner, Z. Phys. **195**, 273 (1966).
[7] D. R. Nelson, Phys. Rev. B **13**, 2222 (1976).
[8] G. F. Mazenko, Phys. Rev. B **14**, 3933 (1976).
[9] A. M. Schorgg and F. Schwabl, Phys. Lett. A **168**, 437 (1992).
[10] A. M. Schorgg and F. Schwabl, Phys. Rev. B **49**, 11682 (1994).
[11] B. I. Halperin, P. C. Hohenberg, and S. Ma, Phys. Rev. Lett. **29**, 1548 (1972); Phys. Rev. B **10**, 139 (1974).
[12] C. De Dominicis, E. Brézin, and J. Zinn-Justin, Phys. Rev. B **12**, 4945 (1975); E. Brézin and C. De Dominicis, Phys. Rev. B **12**, 4954 (1975).
[13] C. De Dominicis, J. Phys. (Paris) Colloq. C **1**, 247 (1976).
[14] H. K. Janssen, Z. Phys. B **23**, 377 (1976); R. Bausch, H. K. Janssen, and H. Wagner, Z. Phys. B **24**, 113 (1976).
[15] I. D. Lawrie, J. Phys. A **14**, 2489 (1981); **18**, 1141 (1985).
[16] U. C. Täuber and F. Schwabl, Phys. Rev. B **46**, 3337 (1992).
[17] U. C. Täuber and F. Schwabl, Phys. Rev. B **48**, 186 (1993).
[18] See *Incommensurate Phases in Dielectrics*, edited by R. Blinc and A. P. Levanyuk (North-Holland, Amsterdam, 1986), Vol. 1 and 2.
[19] R. Walisch, J. Petersson, D. Schüßler, U. Häcker, D. Michel, and J. M. Pérez-Mato, Phys. Rev. B **50**, 16192 (1994).
[20] K.-P. Holzer, J. Petersson, D. Schüßler, R. Walisch, U. Häcker, and D. Michel, Europhys. Lett. **31**, 213 (1995).
[21] B. Topic, U. Haeberlen, and R. Blinc, Phys. Rev. B **40**, 799 (1989).
[22] L. D. Landau and E. M. Lifshitz, *Statistical Physics,* (Pergamon, Oxford, 1980).
[23] P. C. Hohenberg and B. I. Halperin, Rev. Mod. Phys. **49**, 435 (1977).
[24] R. Zeyher and W. Finger, Phys. Rev. Lett. Rev. **49**, 1833 (1982).
[25] P. Martin, E. Siggia, and H. Rose, Phys. Rev. A **8**, 423 (1973).
[26] D. J. Amit, *Field Theory, the Renormalization Group, and Critical Phenomena,* 2nd ed. (World Scientific, Singapore, 1984).
[27] J. Zinn-Justin, *Quantum Field Theory and Critical Phenomena*, 2nd ed. (Clarendon Press, Oxford, 1993).
[28] G. Bonera, F. Borsa, and A. Rigamonti, Phys. Rev. B **2**, 2784 (1970).
[29] S. Žumer and R. Blinc, J. Phys. C **14**, 465 (1981).
[30] J. M. Pérez-Mato, R. Walisch, and J. Petersson, Phys. Rev. B **35**, 6529 (1987).
[31] R. Walisch, J. Petersson, and J. M. Pérez-Mato, Phys. Rev. B **35**, 6538 (1987).
[32] A. Abragam, *Principles of Nuclear Magnetism*, (Clarendon Press, Oxford, 1986).
[33] M. H. Cohen and F. Reif, Solid State Phys. **5**, 322 (1957).
[34] A. Rigamonti, Advances in Physics **22**, 115 (1984).
[35] D. J. Amit and Y. Y. Goldschmidt, Ann. Phys. (N.Y.) **114**, 356 (1978).
[36] R. Schloms and V. Dohm, Nucl. Phys. B **328**, 639 (1989); Phys. Rev. B **42**, 6142 (1990).
[37] E. Frey, U. C. Täuber, and F. Schwabl, Phys. Rev. E **49**, 5058 (1994).
[38] P. Mischo, F. Decker, U. Häcker, K.-P. Holzer, J. Petersson, and D. Michel, Phys. Rev. Lett. **78**, 2152 (1997).
[39] A. P. Levanyuk, Sov. Phys. JETP **36**, 571 (1959)
[40] V. L. Ginzburg, Sov. Phys. Sol. State. **2**, 1824 (1960)
[41] J. Ollivier, J. Etrillard, B. Toudic, C. Ecolivet, P. Bourges, and A. P. Levanyuk, Phys. Rev. Lett. **81**, 3667 (1998).
[42] R. de Souza, M. Engelsberg, and D. J. Pusiol, Phys. Rev.

Lett. **66**, 1505 (1991).
[43] E. Frey and F. Schwabl, Phys. Rev. B **42**, 8261 (1990).

$\nu = 0.6695$	$\eta = 0.033$	$z = 2.024$

TABLE I. Critical exponents in the $O(2)$ symmetric ϕ^4 field theory in three dimensions.[23,27]

ω	k	$\chi_\parallel^{-1}$	$\Im\chi_\parallel^{-1}$
$\omega \to 0$	$k \to 0$	$\propto k$	$\to 0$
$\omega \neq 0$	$k \to \infty$	$\propto k^2$	$\propto k^4$
	$\sqrt{\omega/\lambda} < k < m(1)$	$-i\omega/\lambda + \frac{m(1)^2 \cdot k}{1+af(k)}$	$\propto m(1)^4 k^3$
	$k \leq \sqrt{\omega/\lambda}$	$-i\omega/\lambda + \frac{m(1)^2 \cdot k}{1+af(k)}$	$\propto m(1)^{-2}$
	$k \to 0$	$-i\omega/\lambda + \frac{2k \cdot m(1)^2}{a}$	ω/λ

TABLE II. Different scaling laws for the longitudinal susceptibility. The functions $f(k)$ denote regular functions.

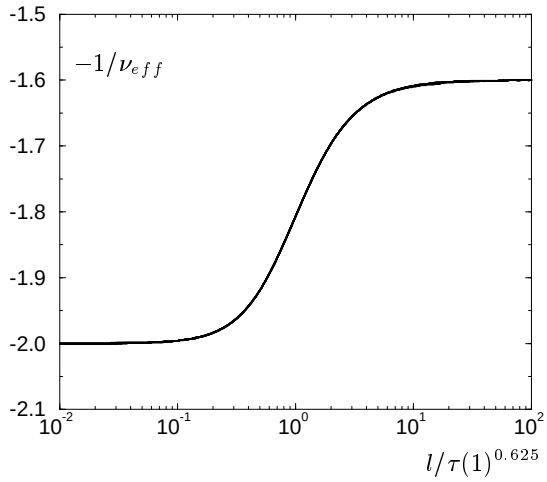

FIG. 1. The flow of the renormalized mass parameter $\tau(l)$ vs. the scaling variable $x = l/\tau(1)^{0.625}$ for ten different values of $\tau(1) < 0.1$ $[u(1) = 0.6, n = 2]$.

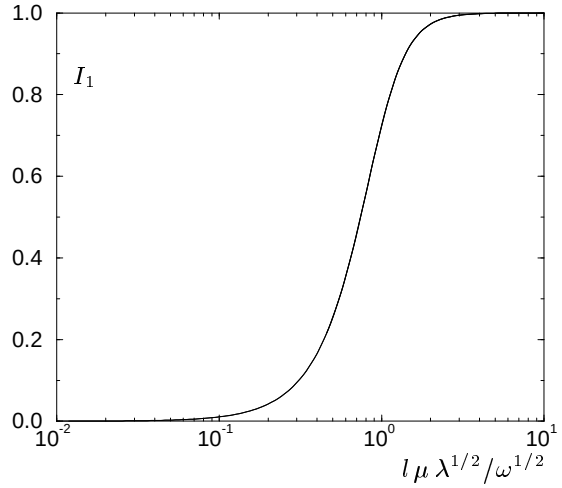

FIG. 2. Logarithmic derivative of the integral in Eq. (4.33) with respect to l, plotted vs. the scaling variable $x = l\mu\lambda^{1/2}/\omega^{1/2}$.

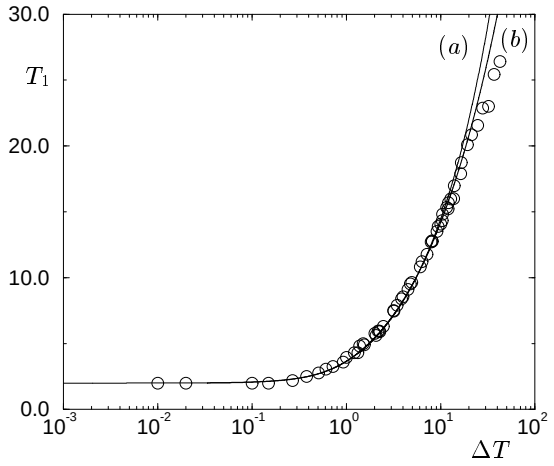

FIG. 3. Relaxation time T_1 vs. the deviation ΔT from the critical temperature T_I. The NMR experimental data,[38] indicated by circles, are compared with the theoretical results, represented by the solid lines. A crossover to the mean-field regime starting at $\Delta T \approx 10K$ [line (a)] and at $\Delta T \approx 5K$ [line (b)] is considered here.

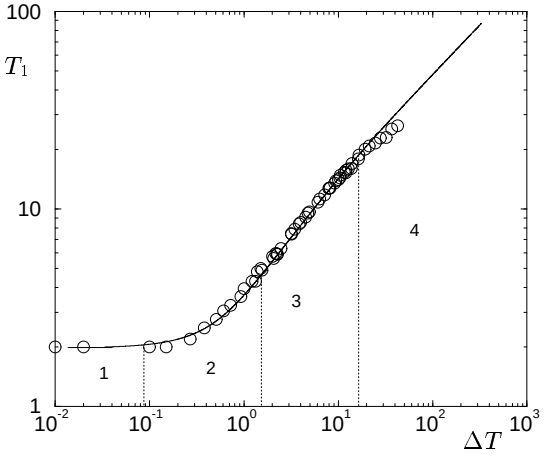

FIG. 4. Relaxation time T_1 in a logarithmic plot vs. the deviation ΔT from the critical temperature T_I. The NMR experimental data[38] (circles) are compared with the theoretical result, represented by the solid line. A crossover to the mean-field regime starting at $\Delta T \approx 5K$ is considered. The four labeled temperature regimes are discussed in the text.

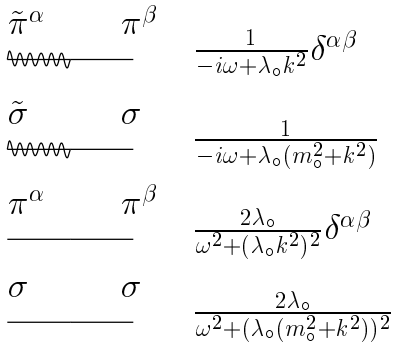

FIG. 5. Propagators below T_I.

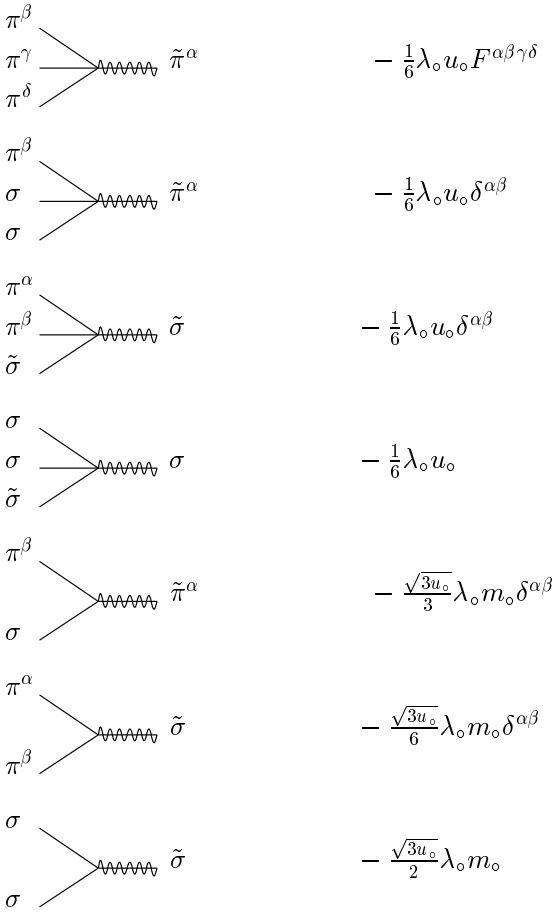

FIG. 6. Vertices below T_I.

$\times$ $A = -\frac{n-1}{6}u_\circ \int_k \frac{1}{k^2} - \frac{1}{2}u_\circ \int_k \frac{1}{m_\circ^2+k^2}$

FIG. 7. Counterterm below T_I.

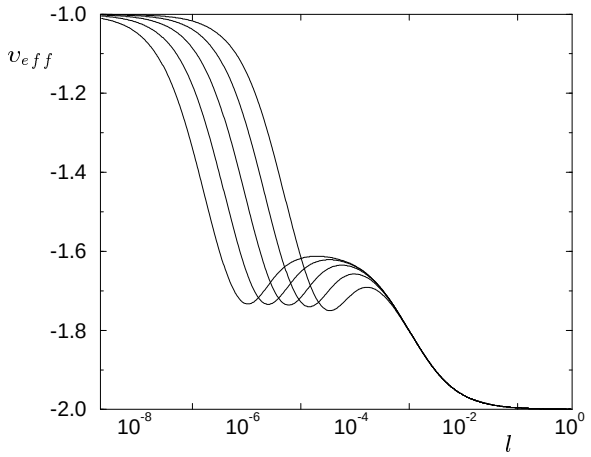

FIG. 8. The effective exponent $v_{eff} = \frac{\partial \log m(l)}{\partial \log l}$ of the flow of the renormalized mass parameter $m(l)$ vs. l for seven different $m(1) \ll 1$ below T_I $[u(1) = 10^{-2} \cdot u_H^*, n = 2, \varepsilon = 1]$

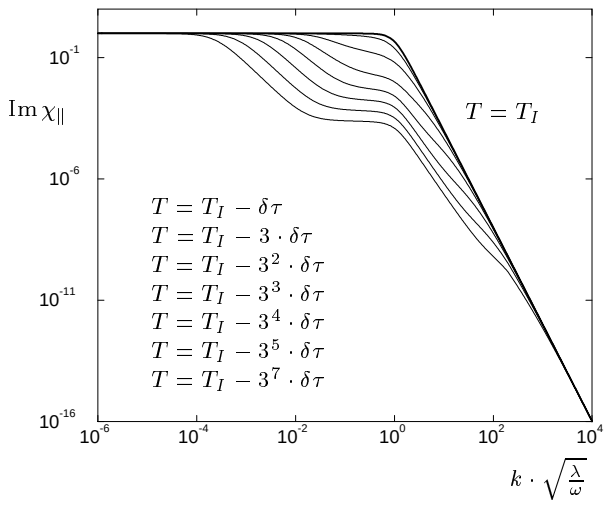

FIG. 10. The longitudinal susceptibility for the critical temperature $T = T_I$ and seven other temperatures plotted vs. $k \cdot \sqrt{\frac{\lambda}{\omega}}$. The scaling regions listed in Table II are valid for temperatures not too close to T_I.

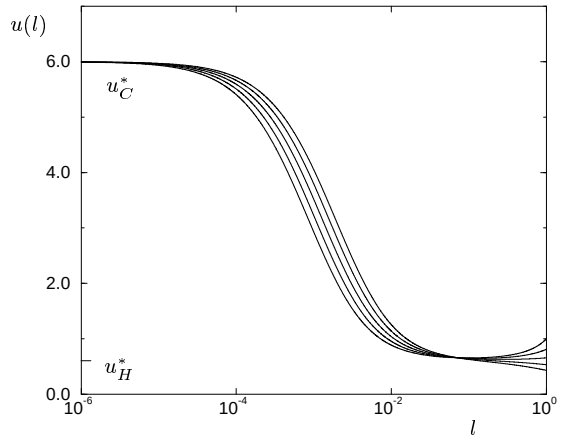

FIG. 9. Flow of the coupling constant $u(l)$ vs. l for five different $u(1)$ below T_I $[m(1) = 0.01, n = 2, \varepsilon = 1]$. The coexistence and the Heisenberg fixed point are marked on the u axis.

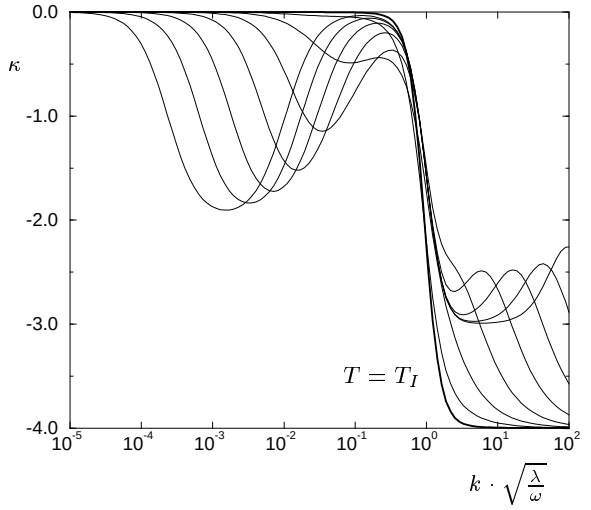

FIG. 11. The effective exponent κ of $\Im\chi_{\parallel}$ with respect to k plotted vs. $k \cdot \sqrt{\frac{\lambda}{\omega}}$ for the same temperatures as in Fig. 10.

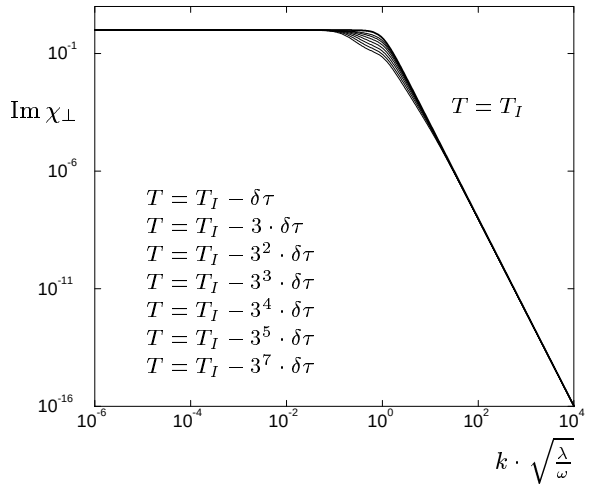

FIG. 12. The transverse susceptibility for the critical temperature $T = T_I$ and seven other temperatures plotted vs. $k \cdot \sqrt{\frac{\lambda}{\omega}}$. The temperature dependence is only present in an interim region.

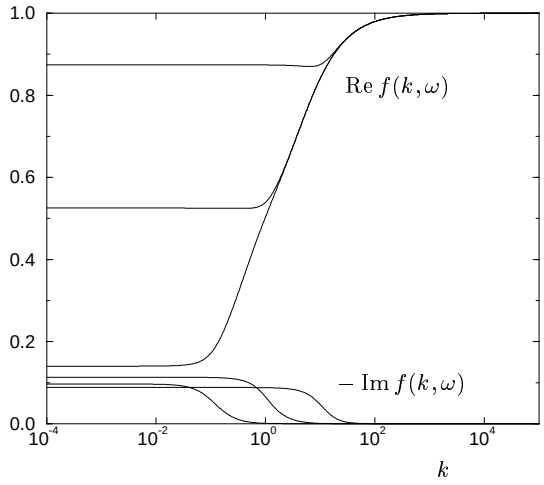

FIG. 14. Real and imaginary part of the effective "mass" (self energy) f and its k dependence for $\tilde{\omega} = 0.01, 1$, and 100.

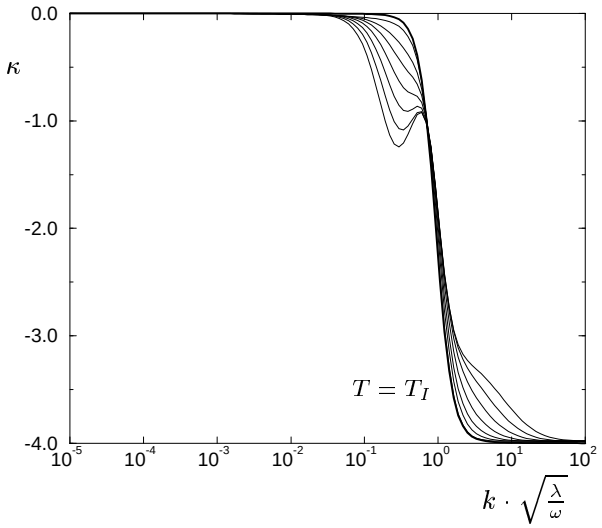

FIG. 13. The effective exponent κ of $\Im\chi_\perp$ with respect to k plotted vs. $k \cdot \sqrt{\frac{\lambda}{\omega}}$ for the same temperatures as in Fig. 12.

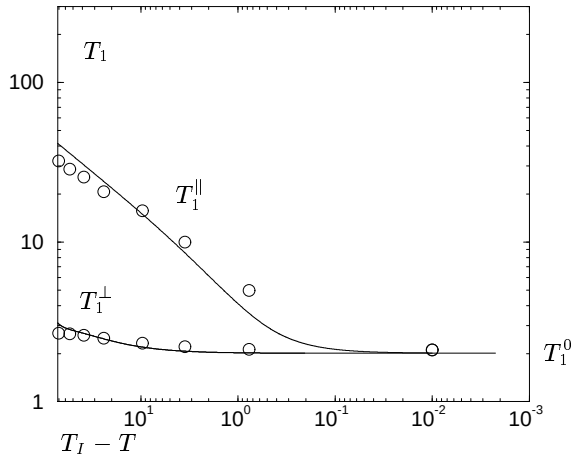

FIG. 15. Relaxation time $T_1^\perp$ (phason dominated) and $T_1^\parallel$ (amplitudon dominated) vs. reduced temperature. The NMR experimental data,[38] again indicated by circles, are compared with the theoretical results, represented by the solid lines. As in the high-temperature phase a crossover to the mean-field regime starting at $\Delta T \approx 5K$ is considered.

$$\lambda_\circ \cdot \chi_\perp^{-1}(-\mathbf{k}, -\omega) = \Gamma_{\circ\tilde{\pi}\pi}(\mathbf{k}, \omega)$$

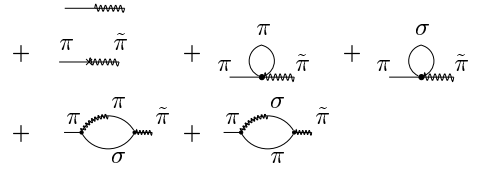

FIG. 16. Transverse susceptibility and its diagrammatic representation.

$$\lambda_\circ \cdot \chi_\parallel^{-1}(-\mathbf{k}, -\omega) = \Gamma_{\circ\tilde{\sigma}\sigma}(\mathbf{k}, \omega)$$

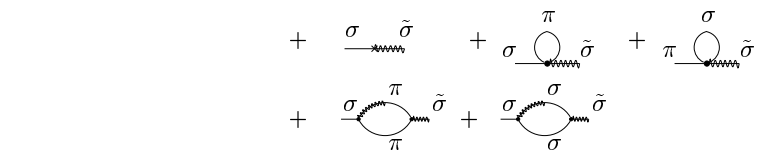

FIG. 17. Longitudinal susceptibility and its diagrammatic representation.